Photospheric Helium Abundance in Cool Giants: A Comprehensive Study

B. P. Hema and Gajendra Pandey

Indian Institute of Astrophysics, Koramangala II Block, Bengaluru, Karnataka-560034, India; hemabp.phy@gmail.com

Received 2025 April 7; revised 2025 June 16; accepted 2025 June 26; published 2025 August 18

Abstract

High-resolution optical spectra of 16 red giants, two early asymptotic giant branch (AGB) stars, and two supergiants, having no/minimal - to super-lithium (Li)-rich abundances, are analyzed to investigate the helium (He)-enhancement. The spectra of eight giants were obtained from the Himalayan Chandra Telescope, and for the rest of the program stars the spectral data were collected from various public archives. Our detailed abundance analyses of the program stars involve the determination of stellar parameters and abundances for about 20 elements among the key abundances of He, Li, C, N, O, and the $^{12}C/^{13}C$ ratios. The difference in the Mg abundance derived from Mg I lines and the MgH band, and the difference in carbon abundance from C I and the CH band, are used as a clue to the mild hydrogen-deficiency/helium-enhancement. From this analysis, four red giants, an early-AGB star, and a supergiant star were found to be enhanced in helium. All these He-enhanced stars are also found to be super-Li rich except for the supergiant. Since the He-rich red giants are Li rich as well, this implies that He enrichment is accompanied by Li enrichment, but not vice versa. This is the first spectroscopic measurement of photospheric He abundance in normal and Li-rich field giants. The Li enrichment is observed across the giant branch from red giant branch (RGB)-bump (KIC 9821622) to AGB phase, unlike that expected from the RGB-tip to red clump phase. A plausible scenario for the enrichment of He as well as Li in giants is the fresh synthesis of Li in the interiors of giants and dredging-up along with He to the surface from deeper layers. However, there could be multiple scenarios operating in tandem. This analysis of He and Li enrichment along with other key elements provides more insights to decipher the mystery of Li enrichment in giants.

Unified Astronomy Thesaurus concepts: Chemical Abundances (224); Helium-rich stars (715); Red Giant Stars (1372); Stellar Evolution (1599)

1. Introduction

Lithium (Li) is one of the key elements in the study of stellar evolution and its observed abundance provides a clue to a star's evolutionary stage (I. J. Iben 1967). Li is a fragile element that can get destroyed at a mere 2.5 million Kelvin. The Li abundance in the atmospheres of main-sequence (MS) stars such as the Sun comes from its primordial material and gradually gets diluted due to the mixing process. As the star evolves to the giant branch, the Li abundance is reduced by about 10–100 times its primordial content. There are a handful of giants that are exceptions to this theory; these giants have a Li abundance of about 1000 times more than that observed in the Sun. The observed abundance of Li in most of the giants is about $\log \epsilon(Li) < 1.5$ dex but in Li-rich giants it ranges between $1.5 < \log \epsilon(Li) < 4.0$ dex (D. L. Lambert et al. 1980; G. Wallerstein & C. Sneden 1982; J. A. Brown et al. 1989; R. G. Gratton & F. D'Antona 1989; R. E. Luck & S. L. Challener 1995; G. Cayrel de Strobel et al. 1997; C. Charbonnel & S. C. Balachandran 2000; N. A. Drake et al. 2002; Y. B. Kumar & B. E. Reddy 2009; B. E. Reddy & D. L. Lambert 2005; R. E. Luck & U. Heiter 2007; Y. B. Kumar et al. 2011; B. F. O. Gonçalves et al. 2020; R. Singh et al. 2020; Y. B. Kumar et al. 2020). The Li-rich stars are mostly low-mass giants with masses $\leqslant 2M_\odot$ with the metallicity ([Fe/H]) ranging from $-0.5 < [Fe/H] < +0.2$. These Li-rich giants are found all across the giant branch of post-MS evolution, i.e., from the base of the red giant branch (RGB), the RGB bump, the RGB, the tip of the RGB, the red clump (RC) phase, and also asymptotic giant branch (AGB) stars.

The source of Li enrichment has been explored for decades. This is yet another study exploring the causes of Li enrichment in giants with a different approach. One such scenario is the fresh production of Li in the giants through the Cameron–Fowler reaction (A. G. W. Cameron & W. A. Fowler 1971) and dredging up to the surface along with the other hydrogen (H)-burnt materials such as helium (He), nitrogen (N), and ^{13}carbon (C). In this study, we explore the He enhancement in the program stars, to investigate if the He and Li enrichment is correlated.

The He enhancement in the cool giants is investigated using our novel and validated method of measuring the accurate He/H ratio from the magnesium (Mg) features, i.e., the Mg I and the subordinate lines of the (0, 0) MgH band. Along with the Mg features and the C features, the C I lines and the CH band were also explored for the determination of He/H ratio. Our sample stars (a random sample) include giants with a range in the abundance of Li, from no/minimal-Li to super-Li-rich abundances from different evolutionary stages of RGB, and two are from the AGB phase. The analyses of the program stars are based on high-resolution optical spectra. By conducting detailed abundance analyses, the elemental abundances for the standard He/H ratio (He/H = 0.1) and also for enhanced He/H ratio are derived. The key elements include He, Li, C, N, O, and the $^{12}C/^{13}C$ ratio. The methodology, analysis, and results are discussed in the following sections. A recent study by A. Mallick et al. (2025) has explored the correlation between high Li abundances and strong chromospheric He I $\lambda 10830$ Å absorption line strengths in Kepler field giant stars, which we discuss in light of our results.

2. Sample Selection, Observations, and Data Reduction

We aim to investigate He enrichment in giants with and without Li enrichment in different stages of their RGB

Table 1
The Program Stars with their Log of Observations

Star	R.A	Decl.	V_{mag}	Obs./Instr.	Date of Obs.	S/N ratio	$R = \lambda/\Delta\lambda$
KIC 9821622	19 08 36.15	+46 41 21.25	12.2	HCT, Hanle	10 Jun 2022	200	30,000
KIC 5184199	19 23 48.42	+40 20 36.18	10.1	HCT, Hanle	9 Apr 2023	200	30,000
KIC 2305930	19 28 25.63	+37 41 23.24	11.0	HCT, Hanle	9 Apr 2023	150	30,000
KIC 12645107	19 17 12.5	+51 45 11.38	11.4	HCT, Hanle	10 Jun 2022	130	30,000
HD 40827	06 05 08.23	+59 23 35.56	6.3	HCT, Hanle	9 Apr 2023	300	30,000
HD 107484	12 21 10.08	+41 28 58.90	7.7	HCT Hanle	9 Apr 2023	250	30,000
HD 233517	08 22 46.71	+53 04 49.23	9.7	HCT Hanle	9 Apr 2023	200	30,000
Ups02 Cas	00 56 39.90	+59 10 51.80	4.6	HCT Hanle	17 Sep 2022	250	30,000
Arcturus	14 15 39.67	+19 10 56.67	−0.05	Mayall Tel. and FTS	1993–94	1000	150,000
HD 77361	09 01 11.41	−26 39 49.37	6.2	McDonald Obs.	25 Dec 2009	300	50,000
HD 214995[a]	22 41 57.45	+14 30 59.01	5.9	OHP-ELODIE	10 Jul 2000	200	42,000
HD 39853[b]	05 54 43.62	−11 46 27.08	5.6	OHP-ELODIE	03 Oct 1996	140	42,000
HD 112127[c]	12 53 55.74	+26 46 47.98	6.9	OHP-ELODIE	27 May 2003	280	42,000
HD 205349[d]	21 33 17.88	+45 51 14.45	6.2	OHP-ELODIE	3 Oct 2003	150	42,000
HD 30834[e]	04 52 25	+36 41 53	4.8	OHP-ELODIE	05 Oct 1996	180	42,000
HD 181475[f]	19 20 48.31	−04 30 09.0	7.0	OHP-ELODIE	02 Jul 2001	170	42,000
HR 334 (HD 81797)	01 08 35.39	−10 10 56.15	3.45	ESO-VLT-U2, UVES	10 Mar 2016	272	115,000
HR 4813 (HD 110014)	12 39 14.76	−07 59 44.04	4.6	ESO-VLT-U2,UVES	10 Mar 2016	356	107,200
HR 6766 (HD 165634)	18 08 04.97	−28 27 25.53	4.5	ESO-FEROS	11 May 2012	300	48,000
HD 19745	03 07 03.24	−65 26 56.80	9.1	ESO-FEROS	7 Dec 2016	110	48,000

Notes. Observer : Program No.
[a] Guillout: Elodie 20000709/0010.
[b] Soubiran: Elodie 19961003/00178.
[c] Liang: Elodie 20030527/0013.
[d] Lebre: Elodie 20031003/0023.
[e] Soubiran: Elodie 19961005/00138.
[f] Catala: Elodie 20010702/0018.

evolution. In total, 20 stars are analyzed in this study. The high-resolution optical spectra for eight program stars are observed from the Himalayan Chandra Telescope (HCT), Hanle. Out of eight giants, four are from the Kepler survey[1] for which the evolutionary states are known by asteroseismology (W. J. Borucki et al. 2010) and the other four are known local giants. For the remaining 12 program stars, the high-resolution spectra were retrieved from the archives of the ELODIE, ESO: UVIT and FEROS, McDonald Observatory and the Kitt Peak Observatory. The observations and the data handling processes are discussed below. The details of the observations are summarized in Table 1.

2.1 The Himalayan Chandra Telescope

High-resolution optical spectra for eight of our program stars were obtained from the HCT, Hanle. The 2 m HCT is mounted with the high-resolution Hanle Echelle Spectrograph (HESP; S. Sriram et al. 2018). HESP is a fiber-fed, cross-dispersed spectrograph that uses a $4\,K \times 4\,K$ CCD covering the complete visible wavelength range from 3700 to 10000 Å providing a resolving power ($R = \lambda/\Delta\lambda$) of 30,000 as well as 60,000. The observations with $R = 30,000$ were carried out between 2022 April and 2023 June (see Table 1). The data reduction and processing were carried out using the IRAF software package.[2] The ThAr lamp and quartz blue lamps were used for wavelength calibration and flat-fielding, respectively. The high-resolution spectra for the

program stars KIC 9821622, KIC 5184199, KIC 2305930, KIC12645107, HD 40827, HD 107484, HD 233517, and Ups02 Cas were obtained from the HCT.

2.2 Elodie Spectrograph–OHP

ELODIE is a fiber-fed cross-dispersed echelle spectrograph installed at the Observatoire de Haute-Provence 1.93m reflector, which has been in operation since 1993. Light from the Cassegrain focus is fed into the spectrograph through a pair of optical fibers. The spectra cover about 3000 Å ranging from 3850 to 6800 Å with a resolving power of ∼42,000, which is recorded on a $1\,K \times 1\,K$ CCD. The instrument is entirely computer-controlled and a standard data reduction pipeline automatically processes the data (J. Moultaka et al. 2004). The spectra of the program stars taken from ELODIE archive[3] are: HD 30834, HD 39853, HD 112127, HD 205349, HD 214995, and HD 181475.

2.3 The UVES and FEROS–ESO

The Ultraviolet and Visual Echelle Spectrograph (UVES) is a high-resolution optical spectrograph of the Very large Telescope installed at the Unit Telescope-2 (UT2) of 4 UTs of 8.2 m diameter of ESO. It is a dual beam, cross-dispersed echelle spectrograph with resolutions of up to $R = 80,000–115,000$. The wavelength coverage is about 1000 Å in the blue arm and about 2000 or 4000 Å in the red arm, with wavelengths between 3200 Å and 10500 Å (H. Dekker et al. 2000). The reduced spectra of the program

---

[1] https://archive.stsci.edu/missions-and-data/kepler
[2] The IRAF software is distributed by the National Optical Astronomy Observatories under contract with the National Science Foundation (D. Tody 1986, 1993).

[3] http://atlas.obs-hp.fr/elodie/

stars HR 334 and HR 4813 were retrieved from the ESO-UVES archives.[4]

The Fiber-fed Extended Range Optical Spectrograph (FEROS; A. Kaufer et al. 1999) is a high-resolution spectrograph installed at the MPG/ESO 2.2 m telescope. It is a fiber-fed visible spectrograph that operates in Cassegrain mode of focus covering wavelengths ranging from 3500 to 9200 Å at a resolving power, $R = 48,000$. The reduced spectra for the program stars HR6766 and HD 19745 were retrieved from the ESO-FEROS archives.

2.4 McDonald Observatory

The high-resolution optical spectrum of the super-Li-rich cool giant HD 77361 was obtained from the McDonald Observatory. The spectrum obtained with the 2.7 m Harlan J. Smith Telescope and Tull coude cross-dispersed echelle spectrograph (R. G. Tull et al. 1995) is at a resolving power of about $R = 50,000$. The spectrum was reduced using the IRAF software package following the standard procedure.

2.5 Kitt Peak Observatory

For our standard-giant star Arcturus, the spectrum was obtained from the Archives of Nicholas U. Mayall 4 m Telescope at Kitt Peak National Observatory. These observations were made with the Coude Feed Telescope on Kitt Peak with the spectrograph in the echelle mode at a resolving power of about $R = 150,000$ with the wavelength coverage of from 3727 to 9300 Å (K. Hinkle et al. 2000).

3. Abundance Analyses

The abundance analyses for all the program stars were conducted using their high-resolution optical spectra obtained as discussed above. To conduct the abundance analyses, the equivalent widths for weak and moderately strong lines of several species that are clean and not severely blended for both neutral and ionized states were measured. The very strong lines were avoided because they are saturated and do not fall in the linear part of the curve of growth. The line list was adopted from B. P. Hema et al. (2018), B. P. Hema & G. Pandey (2020), and B. P. Hema et al. (2020) for which the log gf values were validated using the Solar and the Arcturus spectrum. The new lines included in this work are given in the Appendix. The atomic data for these new lines were adopted from the NIST atomic and molecular database[5] and from B. E. Reddy et al. (2003). The atomic data adopted were also validated by deriving the abundances for Arcturus.

For the determination of stellar parameters and the elemental abundances, the LTE line analysis and spectrum synthesis code MOOG (C. A. Sneden 1973) and the ATLAS9 (R. L. Kurucz 1998) plane parallel, line-blanketed LTE model atmospheres were used. The microturbulence (ξ_t) is derived using Fe I lines having a similar excitation potential and a range in equivalent width, weak to strong, giving the same abundance. The effective temperature ($T_{\rm eff}$) is determined using the excitation balance of Fe I lines having a range in lower excitation potential (LEP). The $T_{\rm eff}$ and ξ_t were fixed iteratively. The process was carried out until both returned zero slope for the derived Fe abundances. By adopting the

determined $T_{\rm eff}$ and ξ_t, the surface gravity (log g) is derived (see Table 2). The log g is fixed by demanding the same abundances from the lines of different ionization states of a species, known as the ionization balance. The log g is derived mainly from the lines of Fe I/Fe II, Ti I/Ti II, and Sc I/Sc II. Since the abundances of Sc I/Sc II are not available for all the stars, the emphasis is mainly given to Fe I/Fe II and Ti I/Ti II. Then, the mean log g was adopted. By adopting these stellar parameters, the abundances were derived for about 23 elements, including the key elements C, N, O, and $^{12}C/^{13}C$ ratios using both the atomic and molecular lines (see Tables 3–9). The details of the line list and the methodology for deriving the C, N, O, abundances and the $^{12}C/^{13}C$ ratios are discussed in the Appendix.

Uncertainties on the $T_{\rm eff}$ and ξ_t are estimated by changing the $T_{\rm eff}$ in steps of 25 K and ξ_t in steps of 0.05 km s^{-1} for the adopted stellar parameters ($T_{\rm eff}$, log g and ξ_t). The change in $T_{\rm eff}$ and ξ_t and the corresponding deviations in abundance, from the zero slope abundance, of about 1σ error, is obtained. This change is adopted as the uncertainty in these parameters. The adopted $\Delta T_{\rm eff} = \pm 50$ K and $\Delta \xi_t = \pm 0.1$ km s^{-1} (see Figure 4 of B. P. Hema & G. Pandey 2020, Section 3). The uncertainty on log g is the standard deviation from the mean value of the log g determined from different species, which is about ± 0.1 (cgs units). The uncertainties adopted on the abundances are the standard deviation of the line-to-line scatter. The uncertainties on the abundances due to the uncertainties on the stellar parameters are < 0.05 dex (B. P. Hema et al. 2018). Since the rms of the errors due to the stellar parameters is less than the line-to-line scatter, the later were adopted.

The non-LTE (NLTE) correction, $\Delta_{\rm NLTE} = \log\epsilon_{\rm NLTE} - \log\epsilon_{\rm LTE}$, ranges from 0.03 to 0.09 dex for various Fe I lines considering electron and H I collisions, and the correction is about 0.01 for Fe II (L. Mashonkina et al. 2011). The Fe I with the excitation energy of the lower level ($E_{\rm LEP}$) < 1 eV, the $\Delta_{\rm NLTE}$ is from 0.04 to 0.09 dex, while $\Delta_{\rm NLTE} = 0.04$ dex is the upper limit for the Fe I lines with $E_{\rm LEP} > 1$ eV. Our line list includes the Fe I lines with the $E_{\rm LEP} > 1$ eV. For Fe I, the NLTE effects on the abundances are expected to be smaller for stars with solar-type metallicities than the metal-deficient stars (M. Bergemann et al. 2012). For this NLTE correction of Fe I lines, the downward revision of the star's adopted $T_{\rm eff}$ by 50 K restores the ionization balance for Fe I/Fe II. This variation in the Fe I and Fe II abundances could also arise due to the uncertainties in the log gf values. However, the adopted uncertainty on the derived Fe abundance for the program stars is the standard deviation of the line-to-line scatter of abundances ($0.07 < \Delta\log\epsilon({\rm Fe\ I}) < 0.16$ dex, except 0.05 dex for Arcturus). This adopted uncertainty is the upper limit and accounts for that due to the stellar parameters and the NLTE corrections. The $\Delta_{\rm NLTE}$ for the Ti I/Ti II abundance is within ≈ 0.02 dex (J. W. E. Mallinson et al. 2022). For the Sc lines, the $\Delta_{\rm NLTE}$ is about -0.06 (L. Mashonkina 2024). The NLTE corrections are significant in very metal-poor dwarfs and giants with [Fe/H] < -2.0 dex. The positive corrections of Fe species and the negative corrections of Sc remove the bias, and our determined $T_{\rm eff}$ and log g are accurate within the uncertainties.

The log g values were also derived by the parallax method and the asteroseismology to support our spectroscopic determination. For the distances derived from the GAIA parallaxes, the log g values were derived using the standard
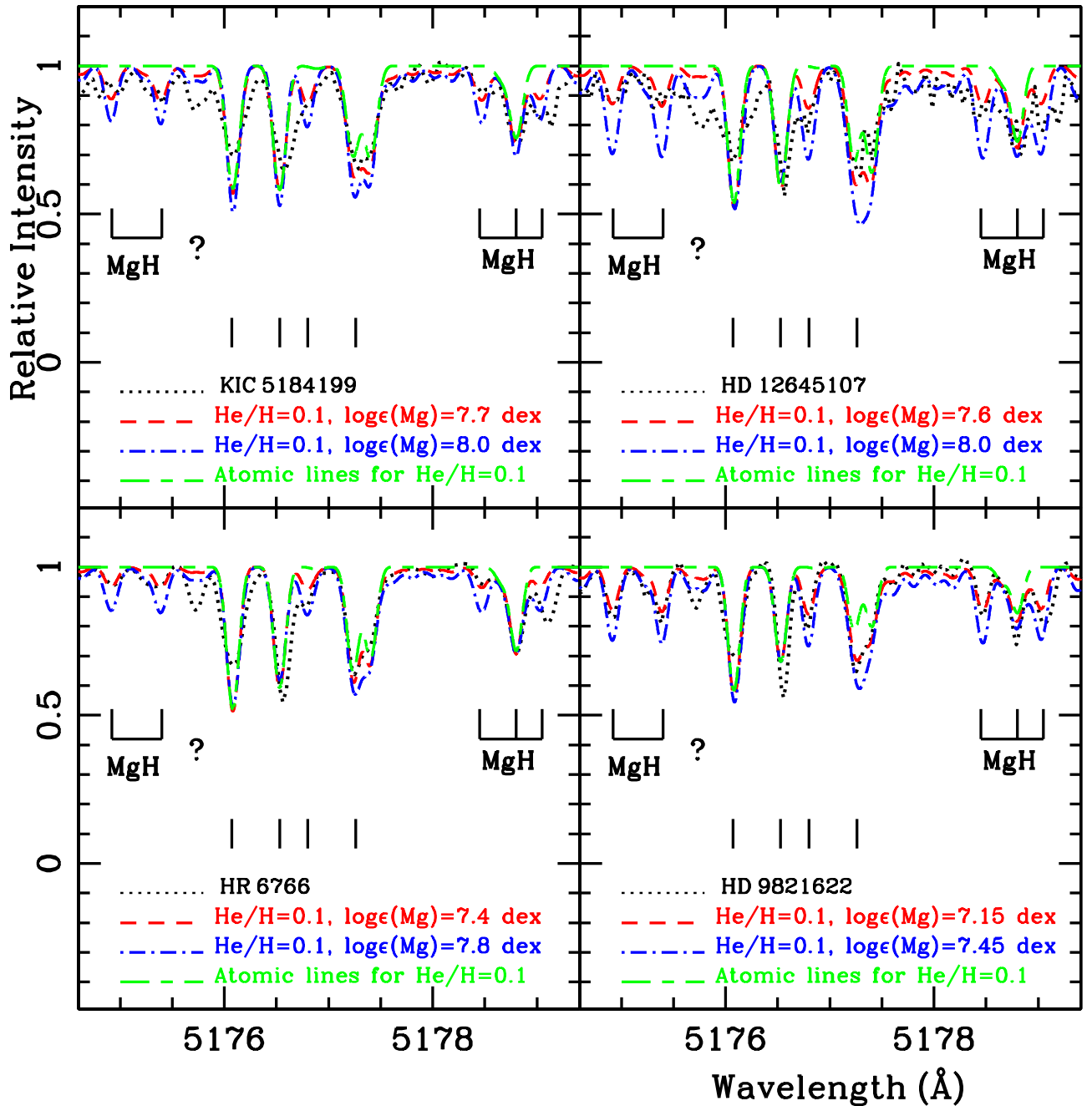

Figure 1. The observed and the synthetic spectra of MgH band. The dotted black line is the observed spectrum of the program star. The best fit synthesized spectrum is shown with dashed red line for the stars' derived He/H ratio (=0.1) and the corresponding Mg abundance (from Mg I and MgH). The synthesis is also shown with dashed–dotted blue line for slightly higher Mg abundance that is not providing the fit. The synthesis for pure atomic lines is shown with the long and short-dashed green line. The MgH lines are marked. The vertical lines are the atomic lines, Co I, Ni I, V I, and Fe I from blue to redward in the spectrum and the question mark is an unknown line.

relation. These log g values agree within 0.1 dex with those derived by us spectroscopically. The log g values were also derived from the seismic parameters; the frequency of maximum oscillation power (ν_{max}) and the large frequency separation ($\Delta\nu$), with the standard relation. For three of the four Kepler field objects of our program stars, the log g values derived by asteroseismology are in excellent agreement with those derived spectroscopically. Hence, the log g values derived from both these methods are in good agreement with the spectroscopic determinations within the adopted uncertainty limits.

4. Spectral Analysis of MgH and CH Bands

4.1. The MgH Band

The He enhancement in the program stars is investigated using the procedure developed by B. P. Hema & G. Pandey (2014), B. P. Hema et al. (2018), and B. P. Hema et al. (2020). The Mg abundance derived from the Mg I lines and from the subordinate lines of the (0, 0) MgH band from the observed stellar spectrum is expected to be same within the uncertainties. In some of our program stars, there is a difference of 0.3 dex or more in the derived Mg abundances from these
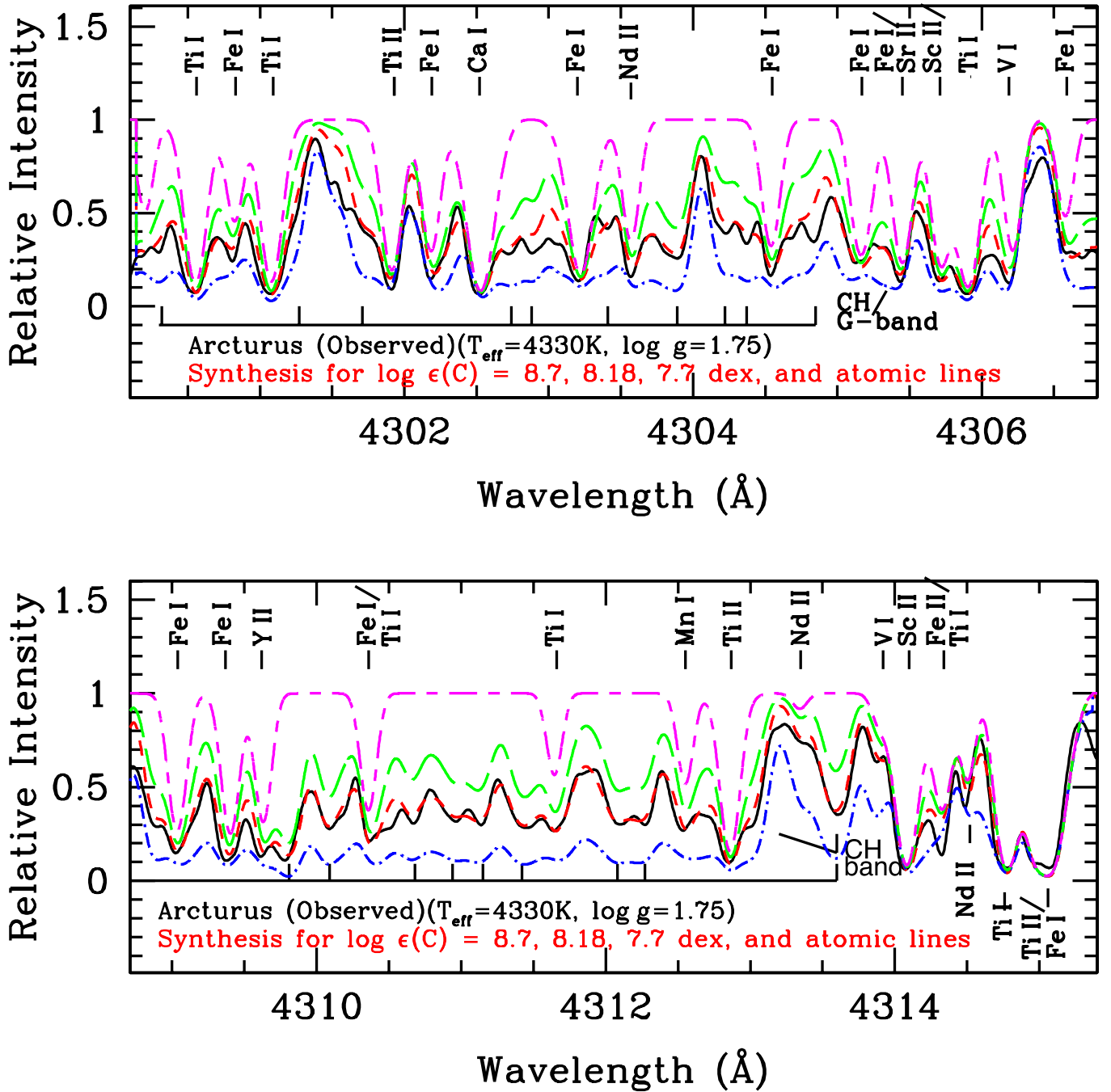
Figure 2. The synthesis of CH band for Arcturus in the two wavelength windows: 4300–4307 Å (top) and 4308–4315 Å (bottom) in comparison with the observed spectrum. The synthesis is shown for three different values of carbon abundances. The syntheses shown are for the best fit (short-dashed line in red) and the other two syntheses are shown with a long-dashed line in green and a dashed–dotted line in blue that are not providing the fit . The magenta line with long- and short-dashed line shows the synthesis for pure atomic lines. The atomic lines and the molecular band are marked.

feature. If this difference is not reconcilable by the uncertainties on the stellar parameters, then it is attributed to the mild H deficiency/He enhancement in the stellar atmosphere.

Spectra of the program stars are synthesized from 5175 to 5179 Å which includes the unblended subordinate lines of the $(0, 0)$ MgH band (see Figure 1 for example). For spectrum synthesis, the atomic lines were compiled from the standard atomic data sources along with those identified by K. Hinkle et al. (2000). The $(0, 0)$ MgH molecular line list was adopted from K. H. Hinkle et al. (2013). Synthetic spectra were

generated by combining the LTE spectral line analysis/synthesis code MOOG (C. A. Sneden 1973) and the ATLAS9 (R. L. Kurucz 1998) plane parallel, line-blanketed LTE model atmospheres with convective overshoot. The spectrum of Arcturus, a typical red giant, was synthesized to validate the adopted *gf* values of the atomic/molecular lines. Using the spectrum synthesis code, *synth* in MOOG, the high-resolution optical spectrum of Arcturus was synthesized for the adopted stellar parameters and the abundances derived by us that agree with those given by I. Ramírez & C. Allende Prieto (2011). The synthesized spectrum was convolved with a Gaussian
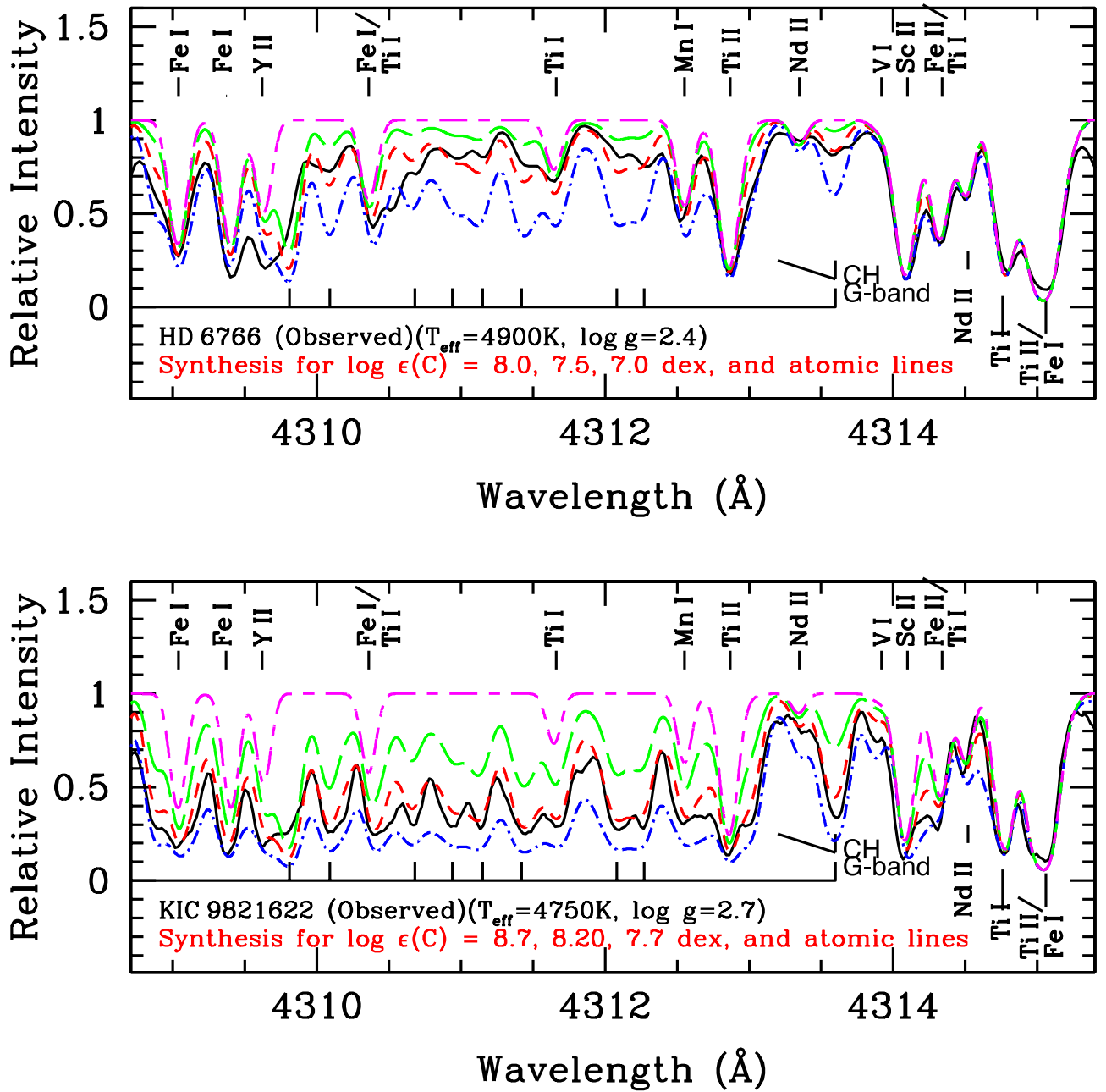
Figure 3. The synthesis of CH band in the wavelength window 4307–4316 Å for the program stars HD 6766 (top panel) and KIC 9821622 (bottom panel) in comparison with the observed spectrum. The synthesis is shown for three different values of carbon abundances. The syntheses shown are for the best fit (short-dashed line in red) and the other two synthesis shown with long-dashed line in green and dashed–dotted line in blue that are not providing the fit . The magenta line with long- and short-dashed line shows the synthesis for pure atomic lines. The atomic lines and the molecular band are marked.

profile with a width that represents the broadening due to macroturbulence and the instrumental profile. Minimal adjustments were made to the abundances of the atomic lines to obtain the best fit to the observed high-resolution optical spectrum of Arcturus (K. Hinkle et al. 2000). The changes in the log *gf* values were not more than 0.1 dex. A reasonably good fit was obtained for the MgH molecular lines for the adopted isotopic values from A. McWilliam & D. L. Lambert (1988). A good match of the synthesized Arcturus spectrum to the observed high-resolution spectra validates the adopted line list for the adopted stellar parameters of Arcturus. These checks on the published analysis of Arcturus are taken as evidence that our implementation of the code MOOG, the LTE

models, and the adopted line list were successful for the syntheses of the spectra of the red giants. Hence, the spectrum of a program star was synthesized following the above procedure. An Mg I line at 5711 Å in the spectra of our program stars is also synthesized to support the Mg abundance derived from the Mg I lines by equivalent width analysis (see the bottom right panel of Figure A1, in the Appendix).

For a program star, the Mg abundance derived from the Mg I lines and from the subordinate lines of the MgH band were compared. If the Mg abundance derived by MgH subordinate lines is <0.3 dex than that derived from the Mg I lines, this difference can be reconciled by changing the stellar parameters within the uncertainties (see Table 2 of B. P. Hema & G. Pandey 2020). And,
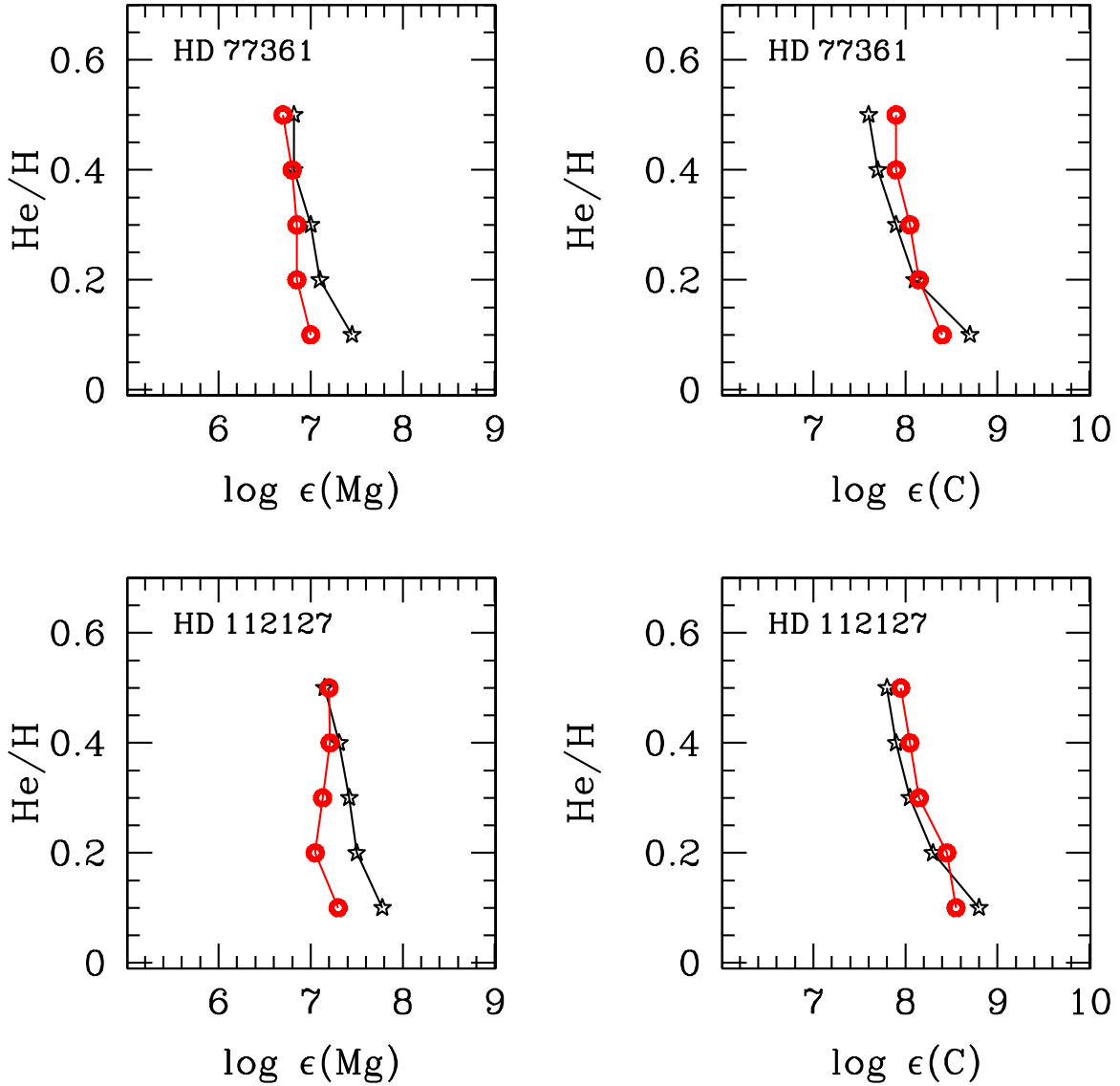
Figure 4. The change in abundance of Mg and C with the He/H ratios. The top panel is shown for the program star HD 77361 and the bottom panel for HD 112127. The left-hand side panels show the change in the Mg abundance derived from the Mg I lines (black stars) and from the MgH band (red dots) for different He/H ratios for these program stars. The right-hand panels show the change in C abundance derived from the C I lines (black stars) and from the CH band (red dots) for different He/H ratios for these program stars.

for some of the program stars, the Mg abundance derived from the MgH bands is less by 0.3 dex or more than that derived from the Mg I lines. This difference ($\geqslant 0.3$ dex) cannot be reconciled by synthesizing the MgH bands by making the changes to the stellar parameters within the uncertainties and also for a slightly higher margin on the uncertainty of the $T_{\rm eff}$. The Mg abundance derived from the MgH band with a change of about ± 100 K on the adopted $T_{\rm eff}$ and the uncertainty on the adopted log g of ± 0.1 also do not provide a comparable Mg abundance from that of the Mg I lines. This difference ($\geqslant 0.3$ dex) in Mg abundance derived from Mg I lines and from the MgH band is unacceptable. Hence, this difference is attributed to the lower H or He enhancement in the atmosphere of the program star. Using the models constructed for differing He/H ratios, the analyses were carried out. The He/H ratios are derived by enforcing the fact that the derived Mg abundances from the Mg I lines and from the subordinate lines of the MgH band must be the same for the adopted model atmosphere and stellar parameters.

As discussed in Section 3, the NLTE correction to the Fe I lines increases the mean Fe abundance by ≈ 0.1 dex. For this change in Fe I abundance, reducing the $T_{\rm eff}$ by about 50 K from adopted is required to restore the ionization balance. With this downward revision of $T_{\rm eff}$, the strength of the synthesized MgH band increases for the Mg abundance derived from the Mg I lines. To match the strength of the synthesized MgH band with the observed, the adopted Mg abundance from Mg I lines has to be decreased further. Hence, increasing the difference in the Mg abundance derived from Mg I lines and the MgH band than that for the adopted stellar parameters from the LTE analysis and making the stars more He enhanced. The determination of the He/H ratio is discussed in detail in the following section.

4.2. The CH Band

In support of our analyses of He enhancement using the Mg features, the C abundance from C I lines and the subordinate

Table 2
The Program Stars in the Order of decreasing $T_{\rm eff}$ with their Stellar Parameters, Log ϵ(Li), He/H Ratio ,and the $v\sin i$ are Given

Star	$T_{\rm eff}$ (K)	Log g (cm s^{-2})	log $L/L_\odot$	$M/M_\odot$	Log ϵ (Li) (dex)	He/H	$v\sin i$ (km s^{-1})
KIC 5184199	5000 ± 50	2.7 ± 0.1	1.59	2.16	<+0.5	0.1	⋯
KIC 12645107	4925 ± 50	2.7 ± 0.1	1.76	1.05 ± 0.04	3.72	0.1	1.5 ± 0.04[b]
HR 6766	4900 ± 50	2.4 ± 0.1	2.20	3.6	1.18	0.1	<5[c]
KIC 9821622	4750 ± 50	2.7 ± 0.1	1.60	1.46	1.54	0.1	1.01[d]
Ups02 Cas	4750 ± 50	2.5 ± 0.1	1.74	⋯	<−0.3	0.1	⋯
KIC 2305930	4725 ± 50	2.5 ± 0.1	1.59	0.92 ± 0.11	4.03	0.4	13.09[e]
HD 19745	4650 ± 50	2.5 ± 0.1	1.65	2.6[a]	4.55	0.1	1.0[f]
HD 40827	4620 ± 50	2.6 ± 0.1	1.80	2.5 ± 0.3	1.87	0.1	1.8[g]
HD 214995	4600 ± 50	2.5 ± 0.1	1.58	⋯	3.27	0.1	4.7 ± 0.3[h]
HDE 233517	4600 ± 50	2.7 ± 0.1	2.18	1.7 ± 0.2	4.24	0.1	17.6[i]
HD 107484	4600 ± 50	2.5 ± 0.1	1.65	0.0	2.10	0.4	⋯
HR 334	4500 ± 50	2.3 ± 0.1	1.84	⋯	1.37	0.1	3.5 ± 0.5[j]
HR 4813	4400 ± 50	2.0 ± 0.1	2.30	⋯	<−0.2	0.1	2.52 ± 0.4[k]
HD 112127	4340 ± 50	2.15 ± 0.1	1.57	1.1 ± 0.2	3.40	0.4	1.6[l]
HD 205349	4330 ± 50	1.7 ± 0.1	3.63	>5	1.92	0.1	⋯
HD 30834	4200 ± 50	1.82 ± 0.1	2.78	4.5 ± 0.3	2.3	0.3	2.7[g]
HD 181475	4100 ± 50	2.3 ± 0.1	3.68	⋯	−0.8	0.5	8.4[g]
HD 39853	4000 ± 50	1.2 ± 0.1	2.77	1.5 ± 0.3	3.90	0.1	3.1[g]
HD 77361	4270 ± 50	2.0 ± 0.1	1.84	1.5 ± 0.2	3.90	0.4	⋯
Arcturus	4330 ± 50	1.75 ± 0.1	2.23	1.1	<−1.0	0.1	3.3[m]

Notes.
[a] L. da Silva et al. (1995).
[b] Y. B. Kumar et al. (2018).
[c] A. Palacios et al. (2016).
[d] R. Singh et al. (2020).
[e] T. Ceillier et al. (2017).
[f] J. R. de Medeiros et al. (1996).
[g] J. R. de Medeiros & M. Mayor (1999).
[h] A. Frasca et al. (2018).
[i] S. C. Balachandran et al. (2000).
[j] M. G. Soto et al. (2021).
[k] E. Jofré et al. (2015).
[l] G. Cayrel de Strobel et al. (1997).
[m] S. B. Borisov et al. (2023).

lines of the CH(G)-band are also explored. Similar to the analyses of Mg features, the analyses of the CH band is carried out by fixing the C abundance accurately from the C I and [C I] lines.

The CH X$^2\pi$–A$^2\delta$ "G band" has strong absorption in the wavelength window λ4200–4400 Å with the band head at 4300 Å. We selected three wavelength regions that have relatively less contamination of atomic lines: λ4300–4308 Å, λ4308–4315 Å, and λ4322–4327 Å. The carbon abundance determined from 4308 to 4315 Å is given more weight because it is less contaminated by atomic lines relative to the other two regions (M. Afşar et al. 2012). For our analysis, the ^{12}CH and ^{13}CH line lists were kindly provided by Prof. Bertrand Plez (through private communications). Using this line list along with the appropriate ATLAS9 model atmospheres and MOOG *synth* code, the spectra were synthesized and matched with the observed spectra. The Arcturus spectrum was synthesized to validate the line list and also the selected spectral regions/spectral lines for a well-determined C abundance (see Figures 2 and 3). For Arcturus, the C abundance derived from the synthesis of the CH band and the C I and [C I] lines are in excellent agreement. Using these methods, the spectra of program stars were analyzed for He enhancement. Since the subordinate lines of ^{12}CH and ^{13}CH are blended, and due to

the lack of pure ^{13}CH lines, the ^{12}C/^{13}C ratio is not estimated from this band.

5. Determination of He/H Ratio

The abundance analyses of the program stars discussed in Section 3 are for normal He/H ratio[6] of 0.1. To derive the He/H ratio for the program stars, the stellar parameters were rederived using a grid of model atmospheres with He/H = 0.15, 0.20, 0.25, 0.30, 0.4, and 0.5. The scripts were written to iterate and generate Kurucz LTE plane-parallel model atmospheres with a fine grid in He/H ratios from the coarse grid of model atmospheres. (Please refer to B. P. Hema et al. 2020 for details of the model atmospheres and the scripts used.)

The input abundances of H and He provided to MOOG, which adopts a model atmosphere computed for a normal He/H ratio of 0.1, are logϵ(H) = 12 and logϵ(He) = 11, respectively. Nevertheless, the input abundances of H and He provided to MOOG are logϵ(H) = 11.894 and logϵ(He) = 11.195, respectively, if a model atmosphere of He/H ratio 0.2 is adopted for analysis.

---

[6] $n_{\rm He}/n_{\rm H}$

Table 3
Elemental Abundances for Program Stars in the Order of their Decreasing T_{eff}

Elements	Sun log $\epsilon(X)_{\odot}$	KIC 5184199 log $\epsilon(X)_{He/H=0.1}$	[X/Fe]	KIC 12645107 log $\epsilon(X)_{He/H=0.1}$	[X/Fe]	HR 6766 log $\epsilon(X)_{He/H=0.1}$	[X/Fe]	KIC 9821622 log $\epsilon(X)_{He/H=0.1}$	[X/Fe]
H	12.00	12.00	⋯	12.00	⋯	12.00	⋯	12.00	⋯
He	10.93	11.00	⋯	11.00	⋯	11.00	⋯	11.00	⋯
Li	1.05	<0.50(1)	−0.50	3.72 ± 0.1(2)	+2.77	1.18(1)	+0.18	1.54(1)	+0.99
C	8.43	8.27 ± 0.04(4)	−0.11	7.88 ± 0.07(3)	−0.45	7.45(1)	−0.93	8.15 ± 0.05(4)	+0.22
CH	8.46	8.40 ± 0.1(3)	−0.01	7.88 ± 0.15(3)	−0.45	>7.0(3)	⋯	8.20 ± 0.03(3)	+0.24
$^{12}C/^{13}C$[a]	89	7 ± 2	⋯	6 ± 2	⋯	>10	⋯	6 ± 1	⋯
N	7.83	8.0 ± 0.1(2)	+0.22	8.30(CN)	+0.57	8.67 ± 0.09(7)	+0.89	8.26 ± 0.12(4)	+0.93
O	8.69	8.87 ± 0.07(6)	+0.23	9.01 ± 0.08(5)	+0.42	8.73 ± 0.09(6)	+0.09	8.84 ± 0.11(6)	+0.65
Na	6.24	6.51 ± 0.07(6)	+0.32	6.30 ± 0.10(3)	+0.16	6.53 ± 0.06(4)	+0.34	5.95 ± 0.03(4)	+0.21
Mg (Mg I)	7.60	7.67 ± 0.08(5)	+0.12	7.60 ± 0.07(5)	+0.10	7.41 ± 0.06(4)	−0.14	7.15 ± 0.07(3)	+0.05
Mg (MgH)	⋯	7.70	+0.15	7.66	+0.16	7.41	−0.14	7.15	+0.05
Al	6.45	6.64 ± 0.08(4)	+0.24	6.41 ± 0.06(4)	+0.06	6.38 ± 0.10(4)	−0.02	6.19 ± 0.06(2)	+0.24
Si	7.51	7.56 ± 0.10(5)	+0.10	7.60 ± 0.08(5)	+0.19	7.61 ± 0.05(5)	+0.15	7.45 ± 0.08(2)	+0.44
Ca	6.34	6.44 ± 0.08(10)	+0.15	6.36 ± 0.10(9)	+0.12	6.20 ± 0.10(8)	−0.09	5.95 ± 0.14(8)	+0.11
Sc I	3.15	⋯	⋯	⋯	⋯	⋯	⋯	⋯	⋯
Sc II	3.15	3.17 ± 0.07(7)	+0.07	3.32 ± 0.06(6)	+0.27	3.16 ± 0.16(6)	+0.06	2.91 ± 0.13(5)	+0.26
Ti I	4.95	5.02 ± 0.08(13)	+0.12	5.04 ± 0.07(11)	+0.19	4.91 ± 0.11(9)	+0.01	4.77 ± 0.08(5)	+0.32
Ti II	4.95	5.03 ± 0.08(4)	+0.13	5.05 ± 0.07(3)	+0.20	4.98 ± 0.14(4)	+0.08	4.72 ± 0.12(4)	+0.27
V	3.93	4.03 ± 0.05(6)	+0.15	3.82 ± 0.08(6)	−0.01	3.85 ± 0.06(6)	−0.03	3.62 ± 0.05(6)	+0.19
Cr	5.64	5.72 ± 0.08(11)	+0.13	5.75 ± 0.06(10)	+0.21	5.61 ± 0.10(10)	+0.02	5.20 ± 0.08(10)	+0.06
Mn	5.43	5.86 ± 0.07(5)	+0.48	5.87 ± 0.06(4)	+0.54	5.33 ± 0.16(4)	−0.05	4.94 ± 0.10(3)	+0.01
Fe I	7.50	7.45 ± 0.09(49)	−0.05	7.40 ± 0.10(39)	−0.10	7.45 ± 0.07(22)	−0.05	7.00 ± 0.10(22)	−0.50
Fe II	⋯	7.46 ± 0.05(12)	−0.04	7.40 ± 0.07(10)	−0.10	7.44 ± 0.02(2)	−0.06	7.00 ± 0.05(2)	−0.50
Co	4.99	4.97 ± 0.07(6)	+0.03	4.96 ± 0.06(6)	+0.07	4.96 ± 0.12(6)	+0.02	4.73 ± 0.12(6)	+0.24
Ni	6.22	6.29 ± 0.07(6)	+0.12	6.16 ± 0.08(5)	+0.04	6.09 ± 0.13(5)	−0.08	5.83 ± 0.14(5)	+0.11
Zn I	4.56	4.66 ± 0.07(2)	+0.15	3.99(1)	−0.47	4.37 ± 0.07(2)	−0.14	4.58 ± 0.07(2)	+0.52
La II	1.10	1.73(1)	+0.68	1.70(1)	+0.70	1.54(1)	+0.49	1.09(1)	+0.49
Eu II	0.52	⋯	⋯	⋯	⋯	0.63(1)	−0.06	0.3(1)	+0.28

Note. The numbers given in parentheses with the abundances are the number of spectral lines of that species used for analysis.
[a] This work

These abundances of H and He for different He/H ratios are calculated by using the standard normalization relation:

$$\sum_{i} \mu_i E_i = \mu_H H + \mu_{He} He + \sum_{i=3} \mu_i E_i = 10^{12.15},$$

where $\mu_i E_i$ represents the total mass of an element E, with atomic number i, with μ_i and E_i denoting the atomic mass and abundance by number for the element E, respectively. Assuming that H and He are the most abundant elements in the stellar atmosphere, while all other elements present are in trace amounts, i.e.,

$$\sum_{i=3} \mu_i E_i \to 0,$$

then $H + 4He = 10^{12.15}$, since $\mu_H = 1$, and $\mu_{He} = 4$. Note that, conventionally, the log of H is $\log \epsilon(H)$ and the log of He is $\log \epsilon(He)$, or, in general log of E is $\log \epsilon(E)$.

The rederived stellar parameters are not sensitive and are almost independent of the adopted grid's He/H ratio. For the adopted stellar parameters of the program stars, the MgH and the CH-band regions were synthesized for different He/H ratios. The Mg and C abundances used for the above syntheses are those derived from the measured equivalent widths of the weak Mg I and C I lines for the adopted model's He/H ratio. Hence, the best fit to the MgH band and the CH band to the observed spectrum determines the adopted model's He/H ratio. Finally, the elemental abundances are derived for the adopted stellar parameters: T_{eff}, log g, ξ_t, and the He/H ratio. Note that the adopted metallicity of the model atmosphere comes from the Fe abundances derived from the measured equivalent widths of the Fe lines for the star in question, and is an iterative process. The results of our analyses with the adoption of α-enhanced model atmospheres having [O/Fe] = 0.5 are in excellent agreement with that of solar-scaled model atmospheres having [O/Fe] = 0.

The elemental abundances derived by adopting the model atmospheres with enhanced He (or He/H > 0.1) are lower than that derived for the normal He/H ratio of 0.1. Here, decreasing the H abundance or increasing the He abundance, i.e., the He/H > 0.1, lowers the continuous opacity per gram (S. Sumangala Rao et al. 2011; B. P. Hema et al. 2020). Hence, for the same observed strength of the spectral line, the elemental abundance has to decrease (refer to Table 4 for example). In Table 4, the abundances derived for the normal He/H ratio of 0.1, and for 0.4 are given for KIC 2305930. The decrease in abundance is proportional to the amount of H deficiency or He enrichment applied in the sense of He/H ratio, except for a few, such as carbon. However, the abundance ratios remain unchanged for most of the elements with few exceptions.

Compared to the MgH band, the CH band is less sensitive to the change in He/H ratio. Therefore, the He/H ratio derived from the MgH band is given more weight. Figure 4 illustrates the variation in Mg abundance from Mg I lines and the MgH

Table 4
Elemental Abundances for Program Stars in the Order of their Decreasing T_{eff}

Elements	Sun log ϵ (X)$_\odot$	Ups02 Cas		KIC 2305930				HD 19745	
		log ϵ(X)$_{He/H=0.1}$	[X/Fe]	log ϵ(X)$_{He/H=0.1}$	[X/Fe]	log ϵ(X)$_{He/H=0.4}$	[X/Fe]	log ϵ(X)$_{He/H=0.1}$	[X/Fe]
H	12.00	12.00	...	12.00	...	11.735	...	12.00	...
He	10.93	11.00	...	11.00	...	11.337	...	11.00	...
Li	1.05	<-0.3	<-0.94	$4.03 \pm 0.08(2)$	+3.36	3.79(2)	+3.49	4.55(1)	+3.50
C	8.43	$8.11 \pm 0.08(4)$	+0.08	$8.11 \pm 0.04(3)$	+0.06	$7.32 \pm 0.1(3)$	-0.36	$8.5 \pm 0.15(3)$	+0.07
CH	8.46	$8.35 \pm 0.15(3)$	+0.29	$8.11 \pm 0.04(3)$	+0.03	$8.05 \pm 0.05(3)$	+0.34	$8.47 \pm 0.06(3)$	+0.01
$^{12}C/^{13}C^a$	89	15 ± 1	...	6 ± 1	...	6 ± 1	...	15[b]	...
N(CN)	7.83	7.7 ± 0.05	+0.27	7.8 ± 0.10	+0.35	7.55	+0.46	7.4 ± 0.06	-0.43
O	8.69	$8.72 \pm 0.1(6)$	+0.43	$9.5 \pm 0.10(5)$	+1.19	$8.81 \pm 0.1(5)$	+0.86	$8.6 \pm 0.14(6)$	-0.09
Na	6.24	$5.80 \pm 0.07(4)$	-0.04	$5.83 \pm 0.10(3)$	-0.03	$5.63 \pm 0.11(3)$	+0.14	$6.21 \pm 0.10(4)$	-0.03
Mg (Mg I)	7.60	$7.26 \pm 0.06(5)$	+0.06	$7.70 \pm 0.08(4)$	-0.48	$7.39 \pm 0.08(4)$	+0.54	$7.40 \pm 0.09(4)$	-0.20
Mg (MgH)	...	7.16	-0.04	7.20	-0.02	7.39	+0.54	7.40	-0.20
Al	6.45	$6.09 \pm 0.06(4)$	+0.04	$6.29 \pm 0.10(4)$	+0.22	$6.00 \pm 0.13(4)$	+0.3	$6.38 \pm 0.08(4)$	-0.07
Si	7.51	$7.23 \pm 0.05(5)$	+0.12	$7.72 \pm 0.08(5)$	+0.59	$7.32 \pm 0.07(5)$	+0.56	$7.65 \pm 0.11(5)$	+0.14
Ca	6.34	$5.85 \pm 0.06(9)$	-0.09	$5.97 \pm 0.09(10)$	-0.01	$5.68 \pm 0.14(10)$	-0.09	$6.16 \pm 0.12(8)$	-0.18
Sc I	3.15	...	...	...	...	...	...	...	...
Sc II	3.15	$2.94 \pm 0.10(7)$	+0.19	$3.03 \pm 0.11(5)$	+0.26	$2.75 \pm 0.13(5)$	+0.35	$3.05 \pm 0.15(6)$	+0.10
Ti I	4.95	$4.43 \pm 0.08(13)$	-0.12	$4.43 \pm 0.11(11)$	-0.14	$4.31 \pm 0.10(10)$	+0.11	$4.83 \pm 0.09(9)$	-0.12
Ti II	4.95	$4.41 \pm 0.09(4)$	-0.14	$4.43 \pm 0.05(4)$	-0.14	$4.17 \pm 0.11(4)$	-0.03	$4.77 \pm 0.05(4)$	-0.18
V	3.93	$3.38 \pm 0.03(6)$	-0.15	$3.54 \pm 0.10(6)$	-0.01	$3.39 \pm 0.12(6)$	+0.21	$3.97 \pm 0.11(6)$	+0.04
Cr	5.64	$5.01 \pm 0.09(11)$	-0.23	$5.65 \pm 0.10(5)$	+0.39	$5.43 \pm 0.12(5)$	+0.00	$5.60 \pm 0.14(10)$	-0.04
Mn	5.43	$4.86 \pm 0.07(4)$	-0.17	$5.29 \pm 0.11(4)$	+0.24	$5.13 \pm 0.10(4)$	+0.45	$5.38 \pm 0.12(4)$	-0.05
Fe I	7.50	$7.09 \pm 0.08(49)$	-0.41	$7.12 \pm 0.11(41)$	-0.38	$6.89 \pm 0.13(41)$	-0.61	$7.50 \pm 0.13(20)$	+0.00
Fe II	7.50	$7.10 \pm 0.07(12)$	-0.40	$7.12 \pm 0.09(10)$	-0.38	$6.64 \pm 0.09(10)$	-0.86	$7.50 \pm 0.06(2)$	+0.00
Co	4.99	$4.49 \pm 0.08(7)$	-0.10	$4.72 \pm 0.11(6)$	+0.11	$4.55 \pm 0.11(6)$	+0.31	$5.08 \pm 0.08(6)$	+0.09
Ni	6.22	$5.82 \pm 0.08(5)$	+0.00	$6.09 \pm 0.11(5)$	+0.25	$5.82 \pm 0.12(5)$	+0.35	$6.18 \pm 0.16(5)$	-0.04
Zn I	4.56	$4.49 \pm 0.03(2)$	+0.33	$4.69 \pm 0.03(2)$	+0.51	$4.26 \pm 0.03(2)$	+0.45	...	...
La II	1.10	1.05(1)	+0.35	0.8(1)	+0.08	0.66(1)	+0.16	1.18(1)	+0.08

Notes. The numbers given in parentheses with the abundances are the number of spectral lines of that species used for analysis.
[a] This work.
[b] R. de La Reza & N. A. Drake (1995), R. de La Reza & L. da Silva (1995), L. da Silva et al. (1995).

band, and C abundance from C I and the CH band with respect to the He/H ratio for the program stars. Once the stellar parameters and metallicity are determined and fixed, the strength of the MgH band primarily depends on the Mg abundance and the He/H ratio. Consequently, the uncertainty in the He/H ratio mainly arises from the uncertainty of the Mg abundance.

6. Program Stars

The program stars were analyzed to explore the He enhancement and its connection to Li enrichment, if any. In this section, He-normal and the He-enhanced giants are discussed in the order of their decreasing T_{eff}.

6.1. He-normal Giants in the Order of Decreasing T$_{eff}$

6.1.1. KIC 5184199

KIC 5184199 is a horizontal branch or RC star for which the evolutionary state is known by asteroseismic studies of the Kepler survey (Kepler Mission Team 2009). The Li I line is weak and only yields an abundance upper limit, logϵ (Li) < 0.5 dex upon synthesis. The derived stellar parameters (refer to Table 2) and elemental abundances (refer to Table 3) agree well with the APOGEE spectral analysis (H. Jönsson et al. 2020; Abdurro'uf et al. 2022). The derived C, N, and $^{12}C/^{13}C$ ratio, along with no detection of Li are as expected for giants. The Mg abundance from Mg I and MgH

band (see Figure 1), and the C abundance from C I and CH band are in excellent agreement for the He/H = 0.1 with no enhancement in He (see Table 10).

6.1.2. KIC 12645107

KIC 12645107 is an RC star as derived from the Kepler survey. The derived stellar parameters (see Table 2) and elemental abundances (see Table 3) agree well with those reported by Y. B. Kumar et al. (2018). The derived Li abundance is about log ϵ(Li) = 3.72 ± 0.1 dex. The star's C, N, and the $^{12}C/^{13}C$ ratio are as expected for first dredge up mixing, except for Li. There is no enhancement of He (see Figure 1); nevertheless, Li is enhanced.

6.1.3. HR 6766

HR 6766 or HD 165634 is a well-studied weak CH(G)-band star (wGb-star). It is an RC star based on its position on the HR diagram. Our determination of stellar parameters (see Table 2) and elemental abundance (see Table 3) agree well with those reported by A. Palacios et al. (2012) and J. Adamczak & D. L. Lambert (2013). The weaker G-band results from a lower C abundance. The derived log ϵ(Li) is 1.18 dex. The C I lines are very weak in the spectrum, and the derived log ϵ(C) is 7.45 dex. Since the CN bands are very weak, the N abundance from N I lines (log ϵ(N) = 8.67 ± 0.09 dex) is adopted, and also yielding only the lower limit to the $^{12}C/^{13}C$ > 10. This is

Table 5
Elemental Abundances for Program Stars in the Order of their Decreasing $T_{\rm eff}$

Elements	Sun $\log \epsilon (X)_\odot$	HD 40827 $\log \epsilon (X)_{\rm He/H=0.1}$	[X/Fe]	HDE 233517 $\log \epsilon (X)_{\rm He/H=0.1}$	[X/Fe]	HD 214995 $\log \epsilon (X)_{\rm He/H=0.1}$	[X/Fe]
H	12.00	12.00	⋯	12.00	⋯	12.00	⋯
He	10.93	11.00	⋯	11.00	⋯	11.00	⋯
Li	1.05	1.87	+0.92	4.24 ± 0.06(2)	+3.44	3.27 ± 0.03(2)	+2.32
C	8.43	8.47 ± 0.06(4)	+0.14	8.25(1)	+0.07	8.5 ± 0.1(1)	+0.17
CH	8.46	8.60 ± 0.15(3)	+0.24	8.3	+0.09	8.5 ± 0.05(3)	+0.17
$^{12}C/^{13}C^a$	89	15 ± 1	⋯	>20 ± 2	⋯	13	⋯
N(CN)	7.83	8.30 ± 0.1	+0.57	8.1	+0.52	8.15 ± 0.1	+0.22
O	8.60	9.07 ± 0.11(6)	+0.48	9.34 ± 0.10(5)	+0.90	8.95 ± 0.1(3)	+0.36
Na	6.24	6.37 ± 0.10(4)	+0.23	5.96 ± .04(2)	−0.03	6.22 ± 0.18(4)	+0.08
Mg (Mg I)	7.60	7.52 ± 0.08(5)	+0.02	7.24 ± 0.06(2)	−0.11	7.26 ± 0.11(3)	−0.24
Mg (MgH)	7.60	7.36	−0.14	7.25	−0.10	7.26	−0.24
Al	6.45	6.48 ± 0.06(4)	+0.13	6.64 ± 0.11	+0.44	6.26 ± 0.05(2)	−0.09
Si	7.51	7.58 ± 0.12(5)	+0.17	⋯	⋯	7.70 ± 0.10(5)	+0.29
Ca	6.34	6.15 ± 0.08(10)	−0.09	5.97 ± 0.12(6)	−0.12	6.11 ± 0.13(6)	−0.13
Sc I	3.15	⋯	⋯	⋯	⋯	3.26 ± 0.13(4)	−0.11
Sc II	3.15	3.08 ± 0.09(7)	+0.03	3.61 ± 0.11(7)	+0.71	3.23 ± 0.11(4)	+0.11
Ti I	4.95	4.80 ± 0.12(13)	−0.05	4.96 ± 0.08(10)	+0.26	4.70 ± 0.07(4)	−0.15
Ti II	4.95	4.70 ± 0.10(4)	−0.15	5.00 ± 0.08(3)	+0.30	4.70 ± 0.16(4)	−0.24
V	3.93	3.85 ± 0.09(6)	+0.02	3.98 ± 0.09(5)	+0.30	3.98 ± 0.14(4)	+0.15
Cr	5.64	5.34 ± 0.09(11)	−0.20	5.24 ± 0.11(7)	−0.15	5.47 ± 0.11(4)	−0.07
Mn	5.43	5.48 ± 0.13(5)	+0.15	5.98 ± 0.04(2)	−0.8	5.39 ± 0.14(3)	+0.06
Fe I	7.50	7.40 ± 0.11(48)	−0.10	7.25 ± 0.10(36)	−0.25	7.4 ± 0.11(19)	−0.10
Fe II	⋯	7.41 ± 0.09(12)	−0.09	7.25 ± 0.11(9)	−0.25	7.40 ± 0.14(7)	−0.10
Co	4.99	5.10 ± 0.13(7)	+0.21	4.63 ± 0.06(5)	−0.11	5.03 ± 0.13(6)	+0.14
Ni	6.22	6.27 ± 0.07(6)	+0.15	6.23 ± 0.10(4)	+0.26	6.23 ± 0.09(3)	+0.11
Zn I	4.56	4.54 ± 0.12(2)	+0.08	3.79(1)	−0.52	⋯	⋯
La II	1.10	1.71(1)	+0.71	1.36(1)	+0.51	1.74(1)	+0.74

Note. The numbers given in parentheses with the abundances are the number of spectral lines of that species used for analysis.

an extreme case of mixing observed in giants with high depletion in C and enhancement in N. Despite the efficient mixing, Li is not destroyed and shows an abundance similar to the Sun ($\log \epsilon$(Li) = 1.05 dex). HR 6766 show no He enhancement (refer to Figure 1 and Table 10).

6.1.4. KIC 9821622

KIC 9821622 is a K-type giant, with a He-inert core, and a confirmed RGB-bump star by the Kepler's asteroseismic data. Our derived stellar parameters (see Table 2) and elemental abundances (see Table 3) agree well with those reported by R. Singh et al. (2020). The N abundances derived from both N I lines and the CN band are the same within the uncertainties and are enhanced as expected for giants. The He/H ratio derived from Mg features (see Figure 1) and CH features (see Figure 3) is 0.1 and He is not enhanced (see Table 10).

6.1.5. Ups02 Cas, HD 19745, HD 40827, and HD 214995

Ups02 Cas is a K giant having no Li with only the upper limit of $\log \epsilon$(Li) < − 0.3 dex (see Table 4). Our determination of stellar parameters and the metallicity are in good agreement with those reported by C. Charbonnel & S. C. Balachandran (2000) and references therein. HD 19745 is at an RGB-bump phase, as shown by its position on the HR diagram with $\log \epsilon$(Li) = 4.55 dex. Our derived stellar parameters (see Table 2) and elemental abundances (see Table 4) are in agreement with those reported by B. E. Reddy & D. L. Lambert (2005) and R. de La Reza & L. da Silva (1995),

within the uncertainties. HD 40827 is an RGB star with $\log \epsilon$(Li) = 1.87 dex. The derived stellar parameters and the elemental abundances (see Table 5) agree well with those reported by R. G. Gratton & F. D'Antona (1989). HD 214995 is a giant star at its RGB-bump phase, as shown by its position on the HR diagram with $\log \epsilon$(Li) = 3.27 ± 0.03 dex. The derived stellar parameters and the elemental abundance (see Table 5) are in excellent agreement with those reported by Y. B. Kumar et al. (2011) and R. E. Luck & U. Heiter (2007).

For all these stars, the derived He/H ratio is 0.1 (see Figure 5) with no enhancement in He (see Table 10).

6.1.6. HDE 233517, HR 334, and HR 4813

HDE 233517 is a super-Li-rich giant at the RGB-bump phase with $\log \epsilon$(Li) = 4.24 dex. The derived stellar parameters and elemental abundances (see Table 5) are in good agreement with those reported by S. C. Balachandran et al. (2000). HR 334 is at an RGB-bump phase with $\log\epsilon$(Li) = 1.37 dex. The derived stellar parameters and elemental abundances (see Table 6) agree with R. E. Luck & S. L. Challener (1995) and D. L. Lambert et al. (1980) within the uncertainties. HR 4813 is a K giant at its RGB-bump phase having a very weak/no detectable Li line, with an upper limit of $\log \epsilon$(Li) < − 0.2 dex. The derived stellar parameters, metallicity, and Li abundances (see Table 6) agree well with those reported by D. L. Lambert et al. (1980). HR 334 and HR 4813 are at the RGB-bump phase but the Li abundances observed are different. The derived He/H ratio is 0.1 for these program stars (see Figure 6) with no He enhancement (see Table 10).
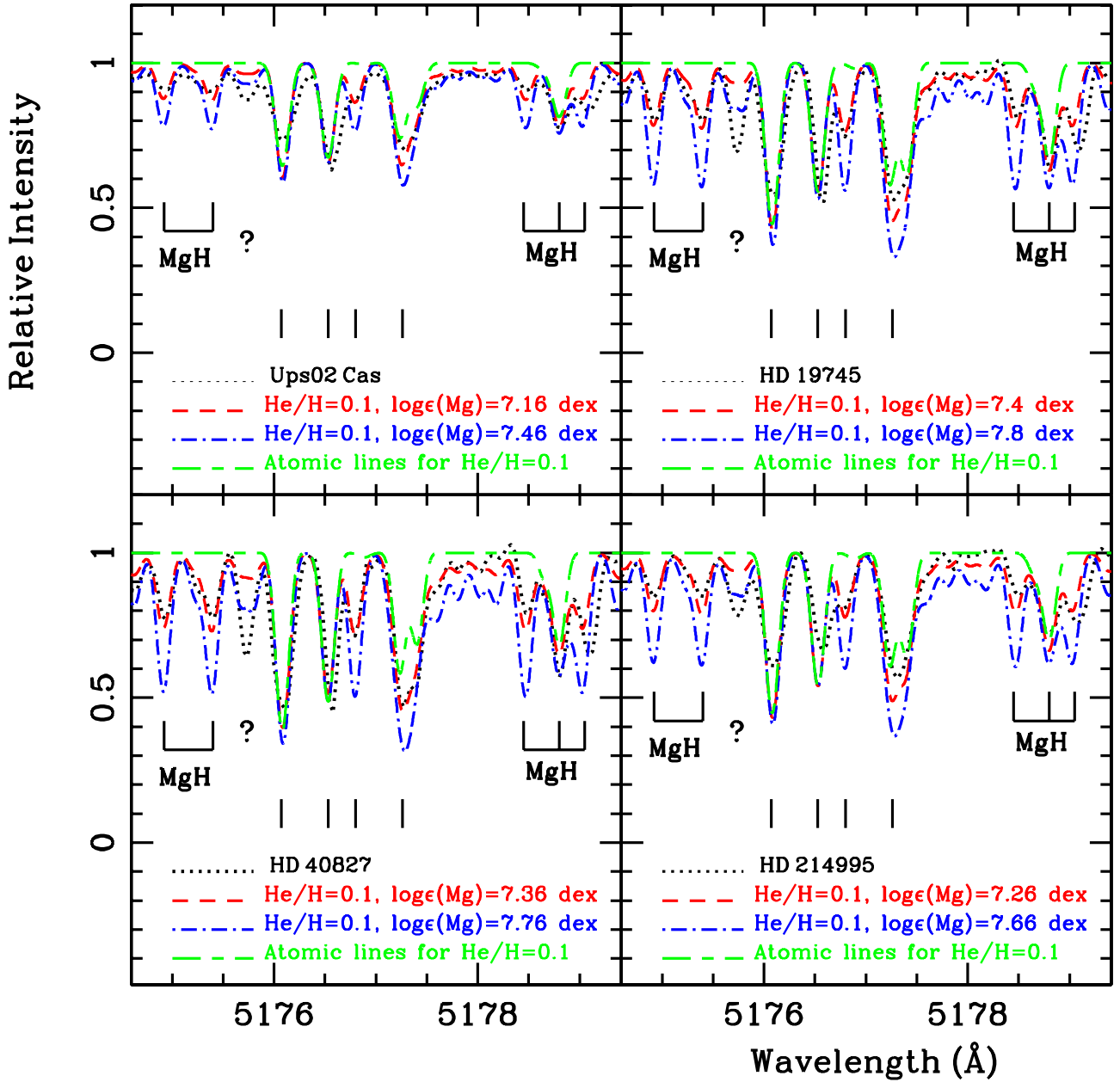
Figure 5. The observed and the synthetic spectra of the MgH band. The dotted black line is the observed spectrum of the program star. The best fit synthesized spectrum is shown with dashed red line for the stars' derived He/H ratio (=0.1) and the corresponding Mg abundance (from Mg I and MgH). The synthesis is also shown with a dashed–dotted blue line for slightly higher Mg abundance that is not providing the fit. The synthesis for pure atomic lines is shown with the long and short-dashed green line. The MgH lines are marked. The vertical lines are the atomic lines, Co I, Ni I, V I, and Fe I from blue to redward in the spectrum and the question mark is an unknown line.

6.1.7. Arcturus, HD 205349, and HD 39853

Arcturus is a standard RGB star with no Li-spectral line in its observed spectrum yielding only the upper limit of $\log \epsilon(\mathrm{Li})$ $< -1.0\,\mathrm{dex}$, as expected for giants. Our derived stellar parameters (see Table 2) and the elemental abundances (Table 7) are in good agreement with those reported by D. L. Lambert & L. M. Ries (1981) and I. Ramírez & C. Allende Prieto (2011), within the uncertainties.

HD 205349 is a probable supergiant star with the derived $\log \epsilon(\mathrm{Li}) = 1.92\,\mathrm{dex}$. The derived stellar parameters and elemental abundances (see Table 7) are in good agreement with those reported by B. F. O. Gonçalves et al. (2020) and J. A. Brown et al. (1989), within the uncertainties. The

observed La abundance of $[\mathrm{La/Fe}] = 0.92\,\mathrm{dex}$ is as expected for a supergiant star. In addition, HD 39853 is a super-Li-rich early-AGB star with Li abundance of $\log \epsilon(\mathrm{Li}) = 3.92\,\mathrm{dex}$. The derived stellar parameters and elemental abundances (see Table 9) are in good agreement with those reported by R. G. Gratton & F. D'Antona (1989).

The derived He/H ratio for these program stars is 0.1 (see Figures 6 and 7) with no He enhancement (see Table 10).

6.2. He-enhanced Giants in the Order of Decreasing T_{eff}

6.2.1. KIC 2305930

KIC 2305930 is an RC star from the Kepler field. This is a super-Li-rich giant with $\log \epsilon(\mathrm{Li}) = 4.03\,\mathrm{dex}$ (see Table 4).

Table 6
Elemental Abundances for Program Stars in the Order of their Decreasing $T_{\rm eff}$

Elements	Sun $\log \epsilon$ $(X)_\odot$	HD 107484 $\log \epsilon (X)_{\rm He/H=0.1}$	[X/Fe]	$\log \epsilon (X)_{\rm He/H=0.4}$	[X/Fe]	HR 334 $\log \epsilon (X)_{\rm He/H=0.1}$	[X/Fe]	HR 4813 $\log \epsilon (X)_{\rm He/H=0.1}$	[X/Fe]
H	12.00	12.00	⋯	11.735	⋯	12.00	⋯	12.00	⋯
He	10.93	11.00	⋯	11.372	⋯	11.00	⋯	11.00	⋯
Li	1.05	2.10 ± 0.07(2)	+1.20	1.80 ± 0.12(2)	+1.25	1.37(1)	+0.28	<−0.2	<−0.9
C	8.43	8.44 ± 0.09(5)	+0.16	7.54 ± 0.13(5)	−0.39	8.65 ± 0.1(2)	+0.18	8.7 ± 0.06(2)	+0.22
C(CH)	8.46	8.50 ± 0.1(3)	+0.19	8.50 ± 0.1(3)	+0.54	8.65 ± 0.04(3)	+0.2	8.75 ± 0.05(3)	+0.21
$^{12}C/^{13}C$	89	20 ± 1	⋯	20 ± 1	⋯	20[a]	⋯	20[a]	⋯
N(CN)	7.83	8.1	+0.42	7.7	+0.37	7.55	−0.32	7.55	−0.33
O	8.69	9.04 ± 0.09(6)	+0.50	8.35 ± 0.2(6)	+0.16	8.85 ± 0.12(3)	+0.12	8.84 ± 0.05(3)	+0.10
Na	6.24	6.48 ± 0.07(4)	+0.39	6.19 ± 0.08(4)	+0.45	6.46 ± 0.13(4)	+0.18	6.63 ± 0.12(4)	+0.34
Mg (Mg I)	7.60	7.46 ± 0.02(5)	+0.01	7.08 ± 0.13(5)	−0.02	7.56 ± 0.05(3)	−0.08	7.61 ± 0.08(3)	−0.04
Mg (MgH)	⋯	7.10	−0.35	7.05	−0.05	7.56	−0.08	7.61	−0.04
Al	6.45	6.50 ± 0.07(4)	+0.20	6.14 ± 0.04(4)	+0.19	6.47 ± 0.05(2)	−0.02	6.58 ± 0.06(2)	+0.08
Si	7.51	7.49 ± 0.11(5)	+0.13	7.06 ± 0.11(5)	+0.05	7.73 ± 0.11(5)	+0.18	7.87 ± 0.09(5)	+0.31
Ca	6.34	6.18 ± 0.09(10)	−0.01	5.78 ± 0.15(10)	−0.06	6.26 ± 0.12(8)	−0.12	6.20 ± 0.08(8)	−0.19
Sc I	3.15	⋯	⋯	⋯	⋯	⋯	⋯	⋯	⋯
Sc II	3.15	3.06 ± 0.12(7)	+0.06	2.74 ± 0.14(7)	+0.09	3.11 ± 0.15(6)	−0.08	3.19 ± 0.10(6)	−0.01
Ti I	4.95	4.80 ± 0.06(12)	+0.00	4.57 ± 0.09(12)	+0.12	4.90 ± 0.11(8)	−0.09	4.97 ± 0.08(8)	−0.03
Ti II	4.95	4.72 ± 0.07(4)	−0.08	4.33 ± 0.07(4)	−0.12	4.85 ± 0.07(3)	−0.14	4.92 ± 0.05(3)	−0.08
V	3.93	4.04 ± 0.08(6)	+0.26	3.71 ± 0.10(6)	+0.28	4.08 ± 0.06(6)	+0.11	4.15 ± 0.10(6)	+0.17
Cr	5.64	5.49 ± 0.09(10)	+0.00	5.23 ± 0.12(10)	+0.09	5.68 ± 0.11(10)	+0.00	5.71 ± 0.11(10)	+0.02
Mn	5.43	5.39 ± 0.01(4)	+0.11	5.15 ± 0.11(4)	+0.22	5.57 ± 0.12(4)	+0.10	5.58 ± 0.05(4)	+0.10
Fe I	7.50	7.35 ± 0.09(48)	−0.15	7.0 ± 0.15(48)	−0.50	7.54 ± 0.13(21)	+0.04	7.55 ± 0.11(21)	+0.05
Fe II	⋯	7.37 ± 0.07(11)	−0.13	6.80 ± 0.12(11)	−0.70	7.55 ± 0.02(2)	+0.05	7.54 ± 0.01(2)	+0.04
Co	4.99	4.90 ± 0.13(7)	+0.06	4.65 ± 0.12(7)	+0.16	5.23 ± 0.14(6)	+0.20	5.34 ± 0.13(6)	+0.30
Ni	6.22	6.41 ± 0.10(4)	+0.34	6.04 ± 0.2(4)	+0.32	6.28 ± 0.15(5)	+0.02	6.39 ± 0.12(5)	+0.12
Zn	4.56	4.47 ± 0.10(2)	+0.06	3.93 ± 0.18(2)	−0.13	⋯	⋯	⋯	⋯
La II	1.10	1.54(1)	+0.59	1.27(1)	+0.67	0.98(1)	−0.16	0.87(1)	−0.28

Note. The numbers given in parentheses with the abundances are the number of spectral lines of that species used for analysis.
[a] R. E. Luck & S. L. Challener (1995).

From the studies of A. Jorissen et al. (2020), KIC 2305930 is a binary star, with $v \sin i = 13\,{\rm km\,s^{-1}}$. The derived stellar parameters and the abundances are in excellent agreement with those reported by Y. B. Kumar et al. (2018).

The Mg abundance derived from the MgH band is about 0.5 dex less than that derived from the Mg I lines, $\log \epsilon({\rm Mg}) = 7.70 \pm 0.08$ dex (see Figure 8). Furthermore, the MgH band synthesized by adopting a model with a He/H ratio of 0.4 and [Fe/H]$_{\rm He}$[7] $= -0.6$ provided the best fit to the observed MgH band for the $\log \epsilon({\rm Mg}) = 7.40$ dex, which is same as that derived from the Mg I lines. For the pair of He/H ratio and [Fe/H], the elemental abundances were derived (see Table 4). The derived Mg abundance from Mg features and C abundance from C features for different He/H ratios are given in Table 10.

6.2.2. HD 107484

HD 107484 is at the tip of the RGB based on its position on the HR diagram, with a Li-rich abundance of $\log \epsilon({\rm Li}) = 2.10$ dex. Our derived stellar parameter and elemental abundances (see Table 6) agree well with those reported by Y. B. Kumar et al. (2011) within the uncertainties. The Mg abundance derived from the MgH band is 0.36 dex less than that derived from the Mg I lines, $\log \epsilon({\rm Mg}) = 7.46$ dex (see Figure 8). Furthermore, the MgH band synthesized for the adopted model with a He/H ratio of 0.4

with [Fe/H]$_{\rm He} = -0.5$ provided the best fit to the observed MgH band for the $\log \epsilon({\rm Mg}) = 7.08$ dex, which is same as that derived from the Mg I lines (see Table 10). For this pair of He/H ratio and [Fe/H], all the elemental abundances are derived (see Table 6).

6.2.3. HD 112127

HD 112127 was the first Li-rich giant discovered by G. Wallerstein & C. Sneden (1982) by the presence of a strong Li-spectral line in its observed spectrum. The derived Li abundance is $\log \epsilon({\rm Li}) = 3.4$ dex. The evolutionary state was determined by asteroseismology using the light curves extracted from TESS FFI[8] (D. A. Caldwell et al. 2020a, 2020b) and it is found to be in RC phase. The derived stellar parameters and the elemental abundances (see Table 7) are in good agreement with those reported by G. Wallerstein & C. Sneden (1982), J. A. Brown et al. (1989), and R. E. Luck & S. L. Challener (1995) within the uncertainties.

The Mg abundance derived from the MgH band is 0.48 dex less than that derived from the Mg I lines, i.e., $\log \epsilon({\rm Mg}) = 7.78$ dex (see Figure 8). Furthermore, the MgH band synthesized by adopting a model with a He/H ratio of 0.4 and [Fe/H]$_{\rm He} = -0.4$ provided the best fit to the observed MgH band for $\log \epsilon({\rm Mg}) = 7.30$ dex, which is same as that derived from the Mg I lines (see Table 10). For this pair of He/H ratio and [Fe/H], all the elemental abundances are derived (see Table 7).

---

[7] [Fe/H]$_{\rm He}$ denotes the metallicity of the He-enhanced giants determined for He-rich models (He/H > 0.1), which derived for the star.

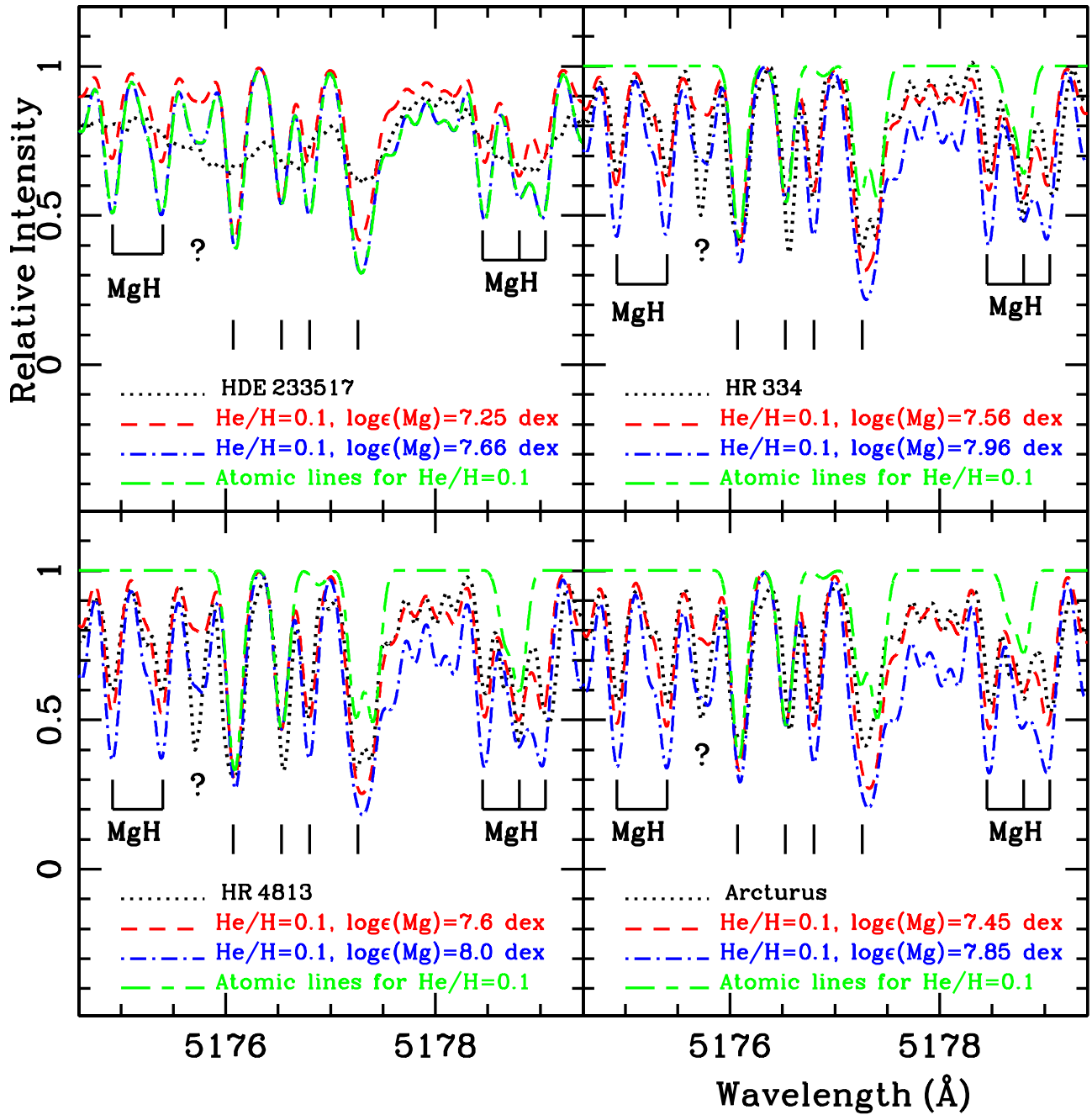[8] https://mast.stsci.edu/portal/Mashup/Clients/Mast/Portal.html

Figure 6. The observed and the synthetic spectra of the MgH band. The dotted black line is the observed spectrum of the program star. The best fit synthesized spectrum is shown with dashed red line for the stars' derived He/H ratio (=0.1) and the corresponding Mg abundance (from Mg I and MgH). The synthesis is also shown with a dashed–dotted blue line for slightly higher Mg abundance that is not providing the fit. The synthesis for pure atomic lines is shown with the long and short-dashed green line. The MgH lines are marked. The vertical lines are the atomic lines, Co I, Ni I, V I, and Fe I from blue to redward in the spectrum and the question mark is an unknown line.

6.2.4. HD 77361

HD 77361 is an RGB-bump star based on its position on the HR diagram with super-Li-rich abundance of $\log\epsilon$ (Li) = 3.9 dex. The determination of stellar parameters and elemental abundances (Table 8) was carried out by B. P. Hema & G. Pandey (2020), and these are in excellent agreement with that reported by L. S. Lyubimkov et al. (2015).

The Mg abundance derived from the MgH band is 0.45 dex less than that derived from the Mg I lines, $\log \epsilon(Mg) = 7.45$ dex (see Figure 8). Furthermore, the MgH band synthesized by adopting a model with a He/H ratio of 0.4 and

$[Fe/H]_{He} = -0.3$ provided the best fit to the observed MgH band for the $\log \epsilon(Mg) = 7.05$ dex, which is same as that derived from the Mg I lines (see Table 10). For the adopted pair of He/H ratio and the [Fe/H], all the elemental abundances are derived (see Table 8).

6.2.5. HD 30834

HD 30834 is an early-AGB star from its position on the HR diagram with Li-rich abundance of $\log \epsilon(Li) = 2.3$ dex. The stellar parameters (see Table 2) and the elemental abundances (see Table 8) derived are in excellent agreement with those

Table 7
Elemental Abundances for Program Stars in the Order of their Decreasing T_{eff}

Elements	Sun $\log \epsilon (X)_{\odot}$	Arcturus $\log \epsilon (X)_{He/H=0.1}$	[X/Fe]	HD 205349 $\log \epsilon (X)_{He/H=0.1}$	[X/Fe]	HD 112127 $\log \epsilon (X)_{He/H=0.1}$	[X/Fe]	$\log \epsilon (X)_{He/H=0.4}$	[X/Fe]
H	12.00	12.00	⋯	12.00	⋯	12.00	⋯	11.735	⋯
He	10.93	11.00	⋯	11.00	⋯	11.00	⋯	11.337	⋯
Li	1.05	<−1.0	<1.43	1.92(1)	1.12	3.40 ± 0.10(2)	+2.28	3.10 ± 0.1(2)	+2.45
C	8.43	8.15 ± 0.07(3)	+0.34	8.6 ± 0.05	+0.42	8.8 ± 0.14(2)	+0.30	7.65 ± 0.07(2)	−0.38
C(CH)	8.46	8.18 ± 0.02(3)	+0.34	8.5 ± 0.1	+0.32	8.60 ± 0.1(3)	+0.07	8.60 ± 0.1(3)	+0.54
^{12}C/^{13}C	89 ± 1	8 ± 1	⋯	⋯	⋯	22[a]	⋯	⋯	⋯
N	7.83	7.45 ± 0.05(CN)	+0.24	7.80 ± 0.05	+0.22	7.85 ± 0.1	−0.05	7.45	+0.02
O	8.69	8.75 ± 0.04(5)	+0.68	8.85 ± 0.08	+0.41	8.95 ± 0.02(3)	+0.19	8.63 ± 0.06(3)	+0.34
Na	6.24	5.77 ± 0.08(4)	+0.15	6.57 ± 0.15(3)	+0.58	6.78 ± 0.18(3)	+0.47	6.43 ± 0.07(3)	+0.59
Mg (Mg I)	7.60	7.48 ± 0.10(5)	+0.50	7.22 ± 0.04(3)	−0.13	7.78 ± 0.05(2)	+0.11	7.32 ± 0.05(2)	+0.12
Mg (MgH)	⋯	7.45	+0.47	7.32	−0.03	7.30	−0.37	7.30	+0.10
Al	6.45	6.23 ± 0.10(4)	+0.40	⋯	⋯	6.14 ± 0.0(2)	−0.38	5.84 ± 0.04(2)	−0.21
Si	7.51	7.20 ± 0.08(5)	+0.31	7.50 ± 0.14(5)	+0.24	7.79 ± 0.19(4)	+0.21	7.27 ± 0.16(4)	+0.13
Ca	6.34	5.93 ± 0.07(10)	+0.21	5.69 ± 0.16(6)	−0.40	6.19 ± 0.15(6)	−0.22	5.83 ± 0.18(6)	-0.11
Sc I	3.15	2.74 ± 0.10(4)	+0.21	3.23 ± 0.11(4)	+0.33	3.62 ± 0.07(2)	+0.40	3.39 ± 0.03(2)	+0.64
Sc II	3.15	2.75 ± 0.07(7)	+0.22	3.27 ± 0.15(5)	+0.37	3.12 ± 0.11(5)	−0.10	2.75 ± 0.10(5)	+0.00
Ti I	4.95	4.64 ± 0.09(13)	+0.31	4.69 ± 0.12(5)	−0.01	4.94 ± 0.13(6)	−0.08	4.73 ± 0.13(6)	+0.18
Ti II	4.95	4.65 ± 0.12(4)	+0.32	4.62 ± 0.12(4)	−0.08	4.88 ± 0.18(2)	−0.14	4.40 ± 0.14(2)	−0.15
V	3.93	3.57 ± 0.09(6)	+0.26	3.86 ± 0.10(4)	+0.18	4.28 ± 0.13(3)	+0.28	4.03 ± 0.13(3)	+0.50
Cr	5.64	5.01 ± 0.12(11)	−0.01	5.36 ± 0.17(5)	−0.03	5.50 ± 0.15(6)	−0.21	5.21 ± 0.15(6)	−0.03
Mn	5.43	4.79 ± 0.12(5)	−0.02	5.07 ± 0.13(3)	−0.11	5.29 ± 0.15(3)	−0.21	5.03 ± 0.19(3)	+0.13
Fe I	7.50	6.88 ± 0.05(50)	−0.62	7.25 ± 0.10(15)	−0.25	7.57 ± 0.16(16)	+0.07	7.10 ± 0.13(16)	−0.40
Fe II	⋯	6.88 ± 0.07(12)	−0.62	7.25 ± 0.09(5)	−0.25	7.57 ± 0.19(6)	+0.07	6.95 ± 0.11(6)	−0.55
Co	4.99	4.74 ± 0.13(7)	+0.37	4.82 ± 0.10(6)	+0.08	5.41 ± 0.16(4)	+0.35	5.02 ± 0.18(4)	+0.29
Ni	6.22	5.76 ± 0.11(6)	+0.16	6.10 ± 0.10(3)	+0.13	6.54 ± 0.15(2)	+0.25	6.06 ± 0.12(2)	+0.24
Zn I	4.56	4.20 ± 0.0(2)	+0.26	⋯	⋯	⋯	⋯	⋯	⋯
La	1.10	1.74(1)	+0.74	1.77(1)	+0.92	1.75(1)	+0.58	1.41(1)	+0.71

Note. The numbers given in parentheses with the abundances are the number of spectral lines of that species used for analysis.
[a] S. V. Berdyugina & I. S. Savanov (1994), R. de La Reza & N. A. Drake (1995), J. A. Brown et al. (1989), G. Wallerstein & C. Sneden (1982).
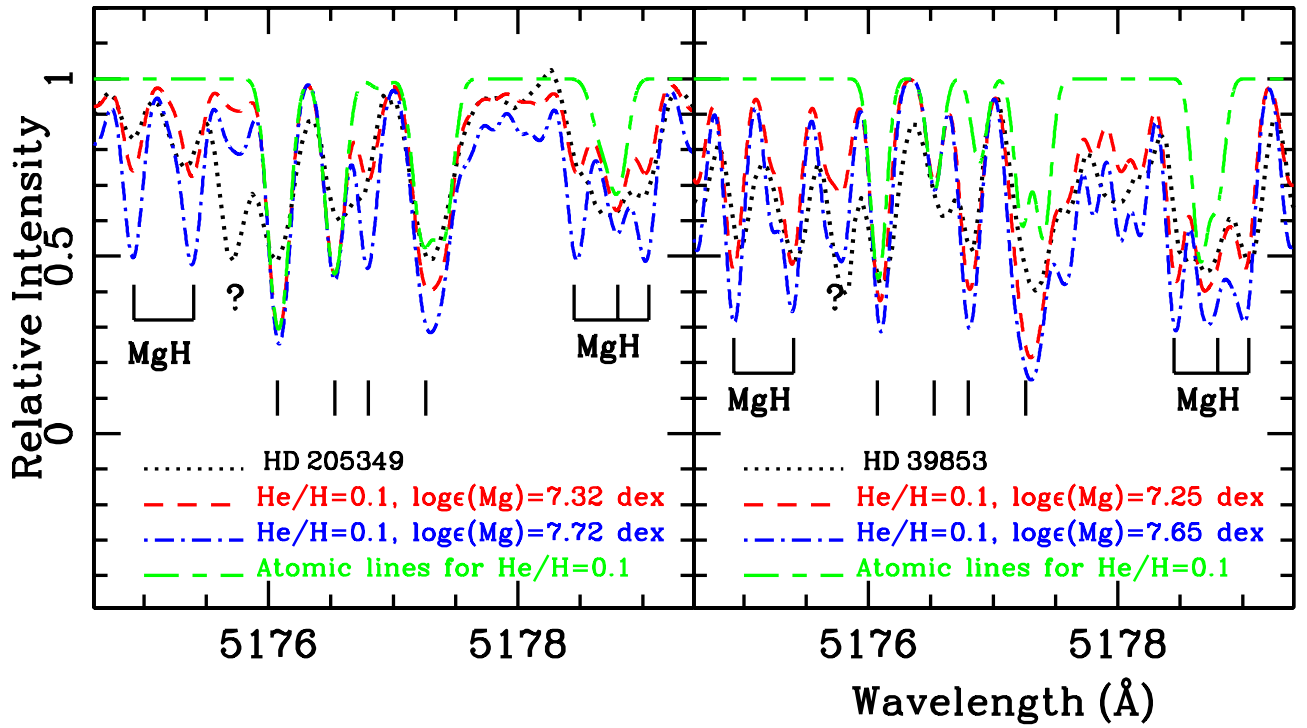
Figure 7. The observed and the synthetic spectra of the MgH band. The dotted black line is the observed spectrum of the program star. The best fit synthesized spectrum is shown with dashed red line for the stars' derived He/H ratio ($=0.1$) and the corresponding Mg abundance (from Mg I and MgH). The synthesis is also shown with a dashed–dotted blue line for slightly higher Mg abundance that is not providing the fit. The synthesis for pure atomic lines is shown with the long and short-dashed green line. The MgH lines are marked. The vertical lines are the atomic lines, Co I, Ni I, V I, and Fe I from blue to redward in the spectrum and the question mark is an unknown line.

reported by G. Cayrel de Strobel et al. (1997) and J. A. Brown et al. (1989).

The Mg abundance derived from the MgH band is about 0.3 dex less than that derived from the Mg I lines, log ϵ(Mg) = 7.28 dex (see Figure 9). Furthermore, the MgH band synthesized by adopting a model for a pair of He/H ratio = 0.3 and $[Fe/H]_{He}$ = −0.45 dex provided the best fit to the observed MgH band for the log ϵ(Mg) = 7.00 dex, which is same as that derived from the Mg I lines (see Table 10). For this pair of He/H and [Fe/H], the elemental abundances are derived (see Table 8).

6.2.6. HD 181475

HD 181475 is a supergiant that has no or very little Li in its atmosphere, yielding only the upper limit of log ϵ(Li) < −0.8 dex, which is in agreement with that reported by N. A. Drake et al. (2002). For the adopted model atmosphere (see Table 2), the elemental abundances are derived (see Table 9).

The Mg abundance derived from the MgH band is about 0.54 dex less than that derived from the Mg I lines, log ϵ(Mg) = 7.54 dex (see Figure 9). Furthermore, the MgH band synthesized by adopting a model with a He/H ratio of 0.5 and $[Fe/H]_{He}$ = −0.3 provided the best fit to the observed MgH band for the log ϵ(Mg) = 7.00 dex, which is same as that derived from the Mg I lines (see Table 10). For the adopted pair of He/H and [Fe/H], the elemental abundances are derived (see Table 9).

7. Results and Discussion

We aim to measure the He enhancement in cool giants with a range in their surface Li abundance from no/minimal to super-Li (about 10 times more than ISM Li). These giants are mostly in the RGB, i.e., from the RGB bump, giant branch, tip of the giant branch and the RC phase. Two of our sample stars are early-AGB and two are supergiant stars that are analyzed for comparison (see Figure 10 of this work and see Figure 1 of I. J. Iben 1967 for an illustrative HR diagram of stellar evolution).

In the MS phase, the nuclear reactions that convert hydrogen to helium in the core are: the proton-proton-chain (pp-chain) reaction and the CN-cycle. Many of our program stars (see Table 2) are of about a solar mass ($M_\odot$) with a few exceptions, in which both pp-chain and CN-cycle operations are expected. The He produced in these reactions and the trace elements such as C, N, etc., that experience abundance changes including the ensuing isotopic ratios are brought to the surface during this dredge up in the RGB phase. The surface Li is diluted during the mixing phase of subgiant and first-ascent red giant evolution. As a result, Li is not expected on the surface of the giants because the temperature involved during the mixing/dredge-up phase is sufficient to destroy Li (I. J. Iben 1967).

From many recent studies, it is observed that about ~1.0% of the known giants are Li rich (R. Smiljanic et al. 2018; Q. Gao et al. 2019; S. L. Martell et al. 2021; Deepak & B. E. Reddy 2022; B. Cai et al. 2023; T. M. Sitnova et al. 2023). One or more processes could be responsible for the Li enrichment in giants, such as preserving the pristine material with which the star is formed, the fresh production, or the contribution of external sources such as Li-rich planet engulfment. We expect that in the Li-rich giants, if the Li is brought to the surface during the first dredge up on the giant branch, it should also be accompanied by He including other key elements. Hence, we expect to find such stars from our
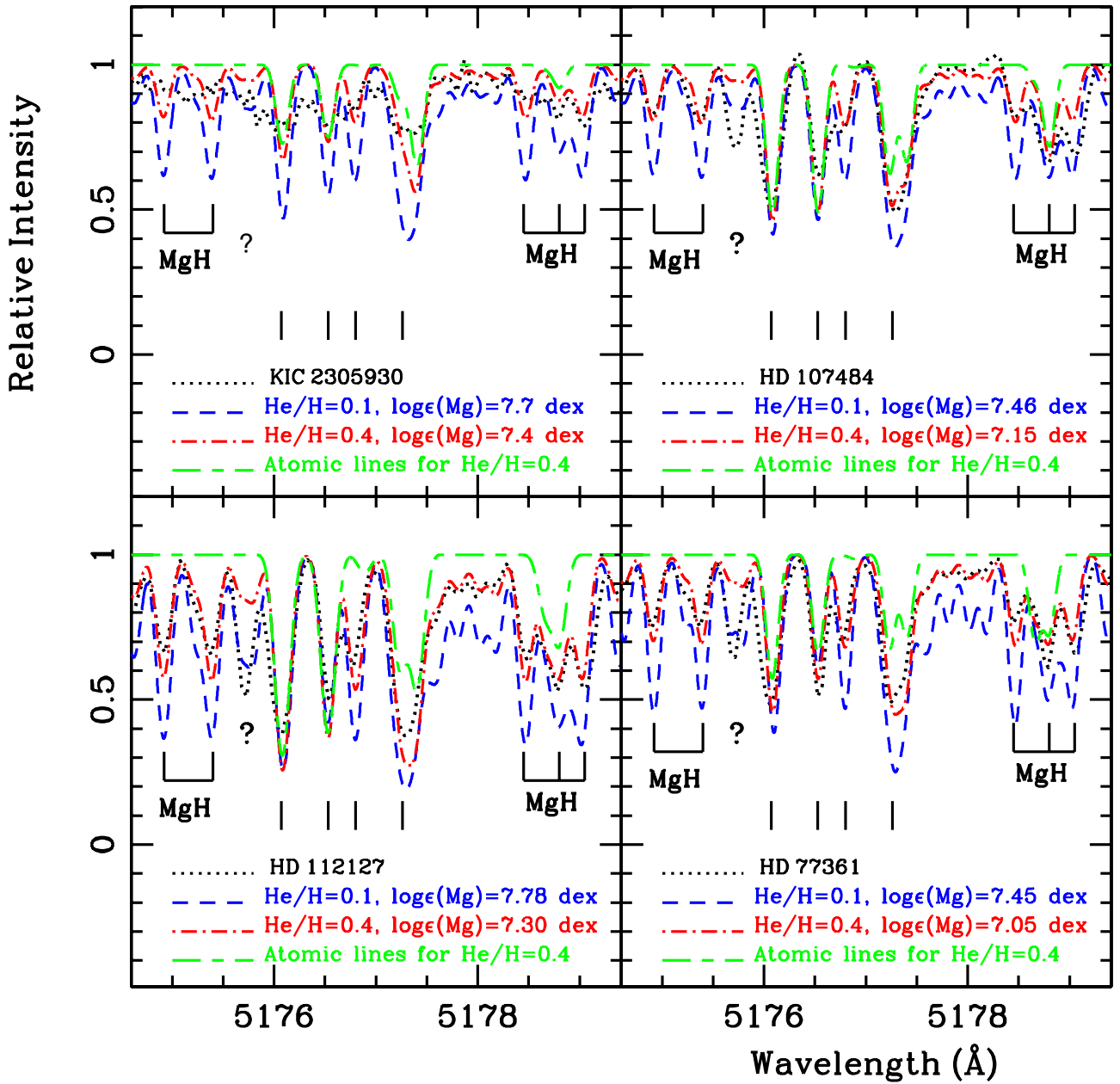
Figure 8. The observed and the synthetic spectra of MgH band. The dotted black line is the observed spectrum of the program star. The dashed–dotted blue line is the synthetic spectrum for the normal He/H ratio of 0.1 and the corresponding Mg abundance (from Mg I). The dashed red line shows the synthetic spectrum for the derived, enhanced He/H ratio, and the corresponding Mg abundance (from Mg I and MgH) that provides the best fit. The synthesis for pure atomic lines is shown with the long and short-dashed green line. The MgH lines are marked. The vertical lines are the atomic lines, Co I, Ni I, V I, and Fe I from blue to redward in the spectrum and the question mark is an unknown line.

sample that are Li as well as He enriched. From our analyses, six stars were found to have a large discrepancy in the derived Mg abundances from the Mg I and MgH lines, and upon syntheses proved to have higher He/H ratios than the standard value of 0.1 (See Section 5) along with super-Li-rich abundances (see Figure 11). The Mg features are the best to determine He/H ratios in giants. However, for MS stars like the Sun, the C features provide more reliable values of He/H ratio (S. Moharana et al. 2024).

Along with the four Kepler field giants in our sample, i.e., KIC 9821622, KIC 12645107, KIC 2305930, and KIC 5184199, an effort was also made to derive the evolutionary states for other program stars using TESS FFI light curves (D. A. Caldwell et al. 2020a, 2020b). Except for HD 112127, which is an RC star (see Figure 12), the evolutionary state could not be derived for any other due to the incomplete data sets or low signal-to-noise ratio. To distinguish between the RGB and the RC giants, R. de la Reza (2025) used the log g values derived using asteroseismic parameters. Adopting the criteria that for the RC giants $2.2 \leqslant \log g \leqslant 2.7$ and for RGB stars $2.8 \leqslant \log g \leqslant 3.5$. Since the spectroscopically derived log g values are in good agreement with those determined from seismic parameters, based on the spectroscopic log g, the evolutionary states are predicted for our He-enhanced giants.
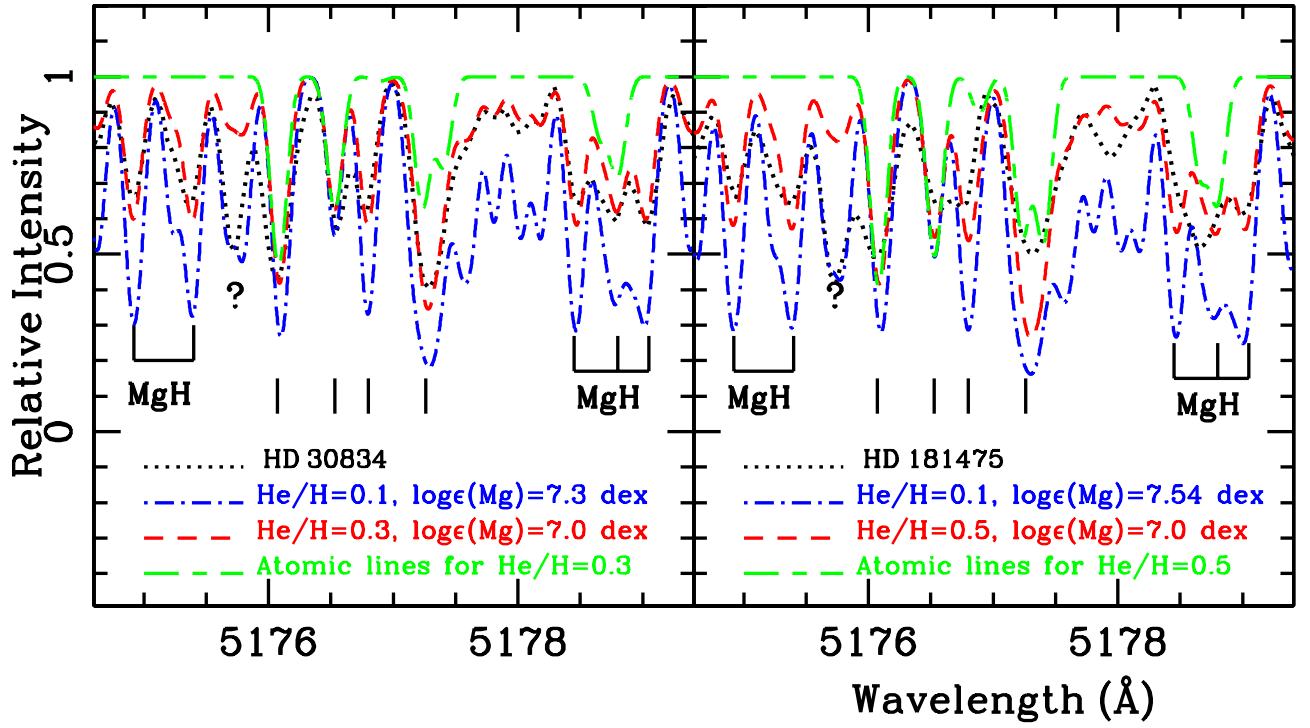
Figure 9. The observed and the synthetic spectra of MgH band. The dotted black line is the observed spectrum of the program star. The dashed–dotted blue line is the synthetic spectrum for the normal He/H ratio of 0.1 and the corresponding Mg abundance (from Mg I). The dashed red line shows the synthetic spectrum for the derived, enhanced He/H ratio, and the corresponding Mg abundance (from Mg I and MgH) that provides the best fit. The synthesis for pure atomic lines is shown with the long and short-dashed green line. The MgH lines are marked. The vertical lines are the atomic lines, Co I, Ni I, V I, and Fe I from blue to redward in the spectrum and the question mark is an unknown.

Table 8
Elemental Abundances for Program Stars in the Order of their Decreasing $T_{\rm eff}$

Elements	Sun $\log \epsilon\,(X)_\odot$	HD 77361 $\log \epsilon\,(X)_{\rm He/H=0.1}$	[X/Fe]	$\log \epsilon\,(X)_{\rm He/H=0.4}$	[X/Fe]	HD 30834 $\log \epsilon\,(X)_{\rm He/H=0.1}$	[X/Fe]	$\log \epsilon\,(X)_{\rm He/H=0.3}$	[X/Fe]
H	12.00	12.00	⋯	11.735	⋯	12.00	⋯	11.735	⋯
He	10.93	11.00	⋯	11.337	⋯	11.00	⋯	11.337	⋯
Li	1.05	3.90(1)	+2.90	3.67(1)	+3.02	2.3 ± 0.1(2)	+1.43	2.1 ± 0.1(2)	+1.50
C	8.43	8.7 ± 0.14(3)	+0.32	7.8 ± 0.02(3)	−0.23	8.18(1)	−0.07	7.55(1)	−0.43
C(CH)	8.46	8.35 ± 0.1(3)	−0.06	8.30 ± 0.1(3)	+0.24	8.25 ± 0.1(3)	−0.03	8.30 ± 0.1(3)	+0.29
^{12}C/^{13}C	89 ± 1	8 ± 1	⋯	8 ± 1	⋯	13[a]	⋯	⋯	⋯
N(CN)	7.83	7.40	−0.38	7.25	−0.18	7.05 ± 0.1	−0.60	6.85 ± 0.1	−0.53
O	8.69	8.75 ± 0.02(2)	+0.06	8.45 ± 0.03(2)	+0.16	8.5 ± 0.07(2)	+0.04	8.41 ± 0.07(2)	+0.18
Na	6.24	6.18 ± 0.05(3)	−0.01	5.89 ± 0.05(3)	+0.05	6.29 ± 0.17(4)	+0.23	6.0 ± 0.13(4)	+0.21
Mg (Mg I)	7.60	7.45 ± 0.13(4)	−0.10	7.05 ± 0.09(4)	−0.15	7.28 ± 0.1(3)	−0.14	7.0 ± 0.06(3)	−0.15
Mg (MgH)	⋯	7.00	−0.55	7.05	−0.15	7.05	−0.37	7.0	−0.15
Al	6.45	6.40 ± 0.08(4)	+0.00	6.05 ± 0.08(4)	+0.00	6.18 ± 0.14(2)	−0.09	5.84 ± 0.05(2)	−0.16
Si	7.51	7.80 ± 0.12(5)	+0.34	7.30 ± 0.11(5)	+0.19	7.47 ± 0.1(2)	+0.14	7.20 ± 0.06(2)	+0.14
Ca	6.34	5.93 ± 0.18(8)	−0.36	5.58 ± 0.17(8)	−0.36	6.15 ± 0.14(7)	−0.01	5.72 ± 0.13(7)	−0.17
Sc I	3.15	2.81 ± 0.13(3)	−0.29	2.69 ± 0.12(3)	−0.06	3.10 ± 0.07(4)	+0.13	2.73 ± 0.07(4)	+0.03
Sc II	3.15	3.00 ± 0.12(5)	−0.10	2.69 ± 0.07(5)	−0.06	2.90 ± 0.1(4)	−0.07	2.80 ± 0.13(4)	+0.10
Ti I	4.95	4.48 ± 0.05(6)	−0.42	4.31 ± 0.06(6)	−0.24	4.78 ± 0.07(4)	+0.01	4.40 ± 0.1(4)	−0.10
Ti II	4.95	4.62 ± 0.08(4)	−0.28	4.24 ± 0.10(4)	−0.31	4.73 ± 0.14(3)	−0.04	4.46 ± 0.14(3)	−0.04
V	3.93	3.56 ± 0.10(4)	−0.32	3.34 ± 0.10(4)	−0.19	3.68 ± 0.11(4)	−0.07	3.25 ± 0.1(4)	−0.23
Cr	5.64	5.32 ± 0.14(7)	−0.27	5.03 ± 0.12(7)	−0.21	5.17 ± 0.16(5)	−0.29	4.80 ± 0.19(5)	−0.39
Mn	5.43	5.30 ± 0.20(3)	−0.08	5.06 ± 0.19(3)	−0.03	5.18 ± 0.16(3)	−0.07	4.94 ± 0.15(3)	−0.04
Fe I	7.50	7.45 ± 0.12(18)	−0.05	7.10 ± 0.12(18)	−0.40	7.32 ± 0.16(15)	−0.18	7.05 ± 0.16(15)	−0.45
Fe II	⋯	7.50 ± 0.05(4)	+0.00	7.00 ± 0.05(4)	−0.50	7.32 ± 0.14(2)	−0.18	7.00 ± 0.14(2)	−0.50
Co	4.99	5.13 ± 0.17(6)	+0.19	4.78 ± 0.17(6)	+0.19	4.89 ± 0.14(6)	+0.08	4.64 ± 0.09(6)	+0.10
Ni	6.22	6.19 ± 0.18(3)	+0.02	5.81 ± 0.13(3)	−0.01	5.86 ± 0.09(2)	−0.18	5.65 ± 0.07(2)	−0.12
La	1.10	2.10(1)	+1.05	1.76(1)	+1.06	2.02(1)	+1.10	1.73(1)	+1.08

Note. The numbers given in parentheses with the abundances are the number of spectral lines of that species used for analysis.
[a] S. V. Berdyugina & I. S. Savanov (1994), R. de La Reza & N. A. Drake (1995).

Table 9
Elemental Abundances for Program Stars in the Order of their Decreasing $T_{\rm eff}$

Elements	Sun $\log \epsilon (X)_\odot$	HD 181475 $\log \epsilon (X)_{\rm He/H=0.1}$	[X/Fe]	$\log \epsilon (X)_{\rm He/H=0.5}$	[X/Fe]	HD 39853 $\log \epsilon (X)_{\rm He/H=0.1}$	[X/Fe]
H	12.00	12.00	⋯	11.673	⋯	12.00	⋯
He	10.93	11.00	⋯	11.372	⋯	11.00	⋯
Li	1.05	<−0.8(1)	−1.96	−1.1(1)	−1.83	3.90 ± 0.03(2)	+3.05
C	8.43	8.7(1)	+0.16	7.70(1)	−0.41	8.50(1)	+0.27
C(CH)	8.46	8.35 ± 0.1	−0.22	8.33 ± 0.1	+0.19	8.5 ± 0.1	+0.24
^{12}C/^{13}C	89±1	⋯	⋯	⋯	⋯	6[a]	⋯
N(CN)	7.83	7.40 ± 0.1	−0.54	7.20 ± 0.1	−0.31	7.5	−0.13
O	8.69	9.1 ± 0.06(2)	+0.30	8.76 ± 0.07(2)	+0.39	8.53 ± 0.05(2)	+0.04
Na	6.24	6.63 ± 0.17(4)	+0.28	6.30 ± 0.25(4)	+0.38	6.20 ± 0.18(4)	+0.16
Mg (Mg I)	7.60	7.54 ± 0.01(3)	−0.17	7.03 ± 0.03(3)	−0.25	7.25 ± 0.04(3)	−0.15
Mg (MgH)	⋯	7.00	−0.71	7.00	−0.28	7.28	−0.12
Al	6.45	6.08 ± 0.11(2)	−0.48	5.75 ± 0.04(2)	−0.38	6.27 ± 0.07(2)	+0.02
Si	7.51	7.85 ± 0.14(4)	+0.23	7.16 ± 0.14(4)	−0.03	7.39 ± 0.1(5)	+0.08
Ca	6.34	5.55 ± 0.19(5)	−0.90	5.20 ± 0.17(5)	−0.82	6.13 ± 0.12(6)	−0.01
Sc I	3.15	⋯	⋯	⋯	⋯	3.02 ± 0.04(2)	+0.07
Sc II	3.15	3.41 ± 0.16(6)	+0.15	3.01 ± 0.17(6)	+0.18	3.00 ± 0.06(3)	+0.05
Ti I	4.95	4.89 ± 0.12(4)	−0.17	4.6 ± 0.12(4)	−0.03	5.31 ± 0.1(4)	+0.56
Ti II	4.95	4.89 ± 0.12(4)	−0.17	4.5 ± 0.10(4)	−0.13	5.17 ± 0.03(3)	+0.42
V	3.93	4.35 ± 0.17(6)	+0.31	4.18 ± 0.2(6)	+0.57	4.52 ± 0.09(4)	+0.80
Cr	5.64	5.42 ± 0.14(6)	−0.33	5.22 ± 0.11(6)	−0.10	5.55 ± 0.13(4)	+0.11
Mn	5.43	5.63 ± 0.12(3)	+0.09	5.41 ± 0.15(3)	+0.30	5.11 ± 0.13(3)	−0.12
Fe I	7.50	7.61 ± 0.16(13)	+0.11	7.18 ± 0.19(13)	−0.32	7.30 ± 0.15(16)	−0.20
Fe II	⋯	⋯	⋯	⋯	⋯	7.28(1)	−0.20
Co	4.99	5.03 ± 0.15(4)	-0.07	4.68 ± 0.14(4)	+0.01	5.05 ± 0.12(4)	+0.26
Ni	6.22	6.47 ± 0.16(3)	+0.14	5.90 ± 0.19(3)	+0.00	5.59 ± 0.03(3)	−0.43
La	1.10	2.63(1)	+1.42	2.28(1)	+1.50	1.16(1)	+0.26

Note. The numbers given in parentheses with the abundances are the number of spectral lines of that species used for analysis.
[a] L. da Silva et al. (1995).

Table 10
A Comparison of Log ϵ(Mg) Derived from the Mg I and MgH Band and, the Log ϵ(C) Derived from the C I and CH band (G band) from the Three Regions

Stars	He/H	$\log \epsilon$(Mg I)	$\log \epsilon$(MgH)	$\log \epsilon$(CI)	$\log \epsilon$(CH[a])	$\log \epsilon$(CH[b])	$\log \epsilon$(CH[c])
KIC 5184199	0.1	7.67	7.70	8.27	8.40	8.40	8.40
	0.2	7.52	7.72	8.09	8.40	8.40	8.40
	0.3	7.45	7.70	7.92	8.35	8.35	8.35
	0.4	7.36	7.72	7.68	8.40	8.40	8.40
	0.5	7.27	7.77	7.40	8.35	8.35	8.35
KIC 12645107	0.1	7.60	7.66	7.88	7.95	7.88	7.90
	0.2	7.42	7.70	7.55	7.85	7.85	7.80
	0.3	7.32	7.70	7.23	7.80	7.80	7.85
	0.4	7.26	7.65	7.10	7.90	7.90	7.85
	0.5	7.21	7.70	6.90	7.85	7.85	7.95
HR 6766	0.1	7.41	7.41	7.45	>7.00	>7.00	>7.0
	0.2	7.26	7.45	7.24	>7.70	>7.70	>7.70
	0.3	7.15	7.40	7.04	>7.70	>7.70	>7.70
	0.4	7.07	7.45	6.90	>7.65	>7.65	>7.65
	0.5	7.01	7.45	6.68	>7.60	>7.60	>7.60
KIC 9821622	0.1	7.15	7.15	8.15	8.20	8.20	8.17
	0.2	7.04	7.20	7.94	8.20	8.15	8.20
	0.3	6.95	7.15	7.68	8.15	8.20	8.20
	0.4	6.89	7.15	7.56	8.20	8.15	8.15
	0.5	6.84	7.20	7.48	8.20	8.20	8.25
Ups02 Cas	0.1	7.26	7.16	8.10	8.30	8.35	8.35
	0.2	7.20	7.10	7.85	8.40	8.30	8.30
	0.3	7.00	7.20	7.72	8.35	8.35	8.40
	0.4	6.92	7.20	7.55	8.30	8.30	8.35
	0.5	6.90	7.15	7.37	8.35	8.30	8.35
KIC 2305930	0.1	7.70	7.20	8.10	8.05	8.10	8.15

Table 10
(Continued)

Stars	He/H	log ϵ(Mg I)	log ϵ(MgH)	log ϵ(CI)	log ϵ(CH[a])	log ϵ(CH[b])	log ϵ(CH[c])
	0.2	7.55	7.25	7.79	8.10	8.10	8.15
	0.3	7.45	7.30	7.55	8.10	8.10	8.20
	0.4	7.39	7.39	7.32	8.00	8.05	8.10
	0.5	7.34	7.40	7.23	8.10	8.10	8.15
HD 19745	0.1	7.40	7.40	8.50	8.47	8.47	8.47
	0.2	7.23	7.40	8.27	8.50	8.50	8.50
	0.3	7.10	7.45	7.90	8.45	8.45	8.45
	0.4	7.03	7.40	7.80	8.45	8.45	8.45
	0.5	6.97	7.40	7.70	8.40	8.45	8.40
HD 40827	0.1	7.52	7.36	8.47	8.60	8.60	8.65
	0.2	7.45	7.35	8.30	8.55	8.50	8.60
	0.3	7.28	7.40	8.10	8.65	8.55	8.55
	0.4	7.20	7.40	7.95	8.60	8.55	8.50
	0.5	7.10	7.40	7.80	8.60	8.55	8.55
HD 214995	0.1	7.26	7.26	8.50	8.50	8.50	8.50
	0.2	7.10	7.30	8.30	8.45	8.45	8.40
	0.3	7.00	7.30	8.16	8.50	8.45	8.45
	0.4	6.92	7.28	8.05	8.45	8.50	8.50
	0.5	6.86	7.25	7.80	8.45	8.45	8.50
HDE 233517	0.1	7.25	7.25	8.25	8.30	8.30	8.25
	0.2	7.15	7.20	8.10	8.25	8.20	8.20
	0.3	7.08	7.25	7.95	8.28	8.20	8.15
	0.4	6.92	7.25	7.83	8.20	8.15	8.23
	0.5	6.85	7.25	7.70	8.30	8.20	8.25
HD 107484	0.1	7.46	7.10	8.44	8.55	8.50	8.44
	0.2	7.30	7.10	8.11	8.52	8.45	8.54
	0.3	7.16	7.00	7.86	8.50	8.45	8.54
	0.4	7.08	7.05	7.54	8.50	8.50	8.54
	0.5	6.85	6.95	7.35	8.52	8.42	8.54
HR 334	0.1	7.56	7.56	8.65	8.65	8.65	8.65
	0.2	7.37	7.56	8.34	8.65	8.65	8.65
	0.3	7.24	7.56	8.03	8.55	8.55	8.55
	0.4	7.18	7.45	7.82	8.56	8.56	8.56
	0.5	7.11	7.45	7.62	8.55	8.55	8.55
HR 4813	0.1	7.61	7.61	8.70	8.75	8.75	8.75
	0.2	7.41	7.60	8.38	8.75	8.75	8.75
	0.3	7.28	7.60	8.05	8.75	8.75	8.75
	0.4	7.21	7.60	8.04	8.65	8.65	8.65
	0.5	7.14	7.60	7.93	8.65	8.65	8.65
HD 112127	0.1	7.78	7.30	8.80	8.55	8.60	8.55
	0.2	7.60	7.30	8.55	8.60	8.55	8.55
	0.3	7.45	7.25	7.95	8.55	8.60	8.55
	0.4	7.32	7.30	7.65	8.55	8.60	8.55
	0.5	7.15	7.35	7.40	8.50	8.60	8.5
Arcturus	0.1	7.48	7.45	8.15	8.18	8.18	8.18
	0.2	7.30	7.43	8.00	8.16	8.16	8.16
	0.3	7.15	7.42	7.87	8.13	8.13	8.13
	0.4	7.00	7.42	7.72	8.13	8.13	8.13
	0.5	6.80	7.40	7.50	8.12	8.12	8.12
HD 205349	0.1	7.22	7.32	8.60	8.50	8.50	8.50
	0.2	7.03	7.25	8.20	8.45	8.45	8.45
	0.3	6.94	7.25	7.90	8.35	8.40	8.35
	0.4	6.86	7.30	7.70	8.35	8.35	8.35
	0.5	6.80	7.25	7.60	8.40	8.35	8.35
HD 77361	0.1	7.45	7.00	8.70	8.40	8.35	8.40
	0.2	7.30	7.10	8.40	8.35	8.35	8.40
	0.3	7.15	7.05	8.10	8.35	8.30	8.35
	0.4	7.05	7.05	7.80	8.30	8.30	8.35
	0.5	6.92	7.05	7.60	8.25	8.35	8.30
HD 30834	0.1	7.28	7.05	8.18	8.25	8.25	8.25
	0.2	7.16	7.00	7.80	8.20	8.20	8.20
	0.3	7.00	7.00	7.55	8.25	8.30	8.25
	0.4	6.87	6.96	7.30	8.25	8.25	8.25
	0.5	6.71	6.96	7.10	8.25	8.25	8.20

Table 10
(Continued)

Stars	He/H	log ϵ(Mg I)	log ϵ(MgH)	log ϵ(CI)	log ϵ(CH[a])	log ϵ(CH[b])	log ϵ(CH[c])
HD 181475	0.1	7.54	7.00	8.70	8.35	8.35	8.40
	0.2	7.40	7.10	8.35	8.30	8.30	8.30
	0.3	7.27	7.10	8.15	8.30	8.30	8.30
	0.4	7.16	7.06	7.95	8.25	8.30	8.25
	0.5	7.03	7.00	7.70	8.33	8.33	8.33
HD 39853	0.1	7.25	7.28	8.50	8.50	8.50	8.50
	0.2	6.97	7.25	8.20	8.45	8.45	8.45
	0.3	6.87	7.20	7.95	8.50	8.50	8.50
	0.4	6.77	7.25	7.75	8.40	8.40	8.40
	0.5	6.69	7.20	7.52	8.45	8.45	8.45

Notes.
[a] The synthesis of CH band in the wavelength window 4300–4308 Å.
[b] The synthesis of CH band in the wavelength window 4308–4315 Å.
[c] The synthesis of CH band in the wavelength window 4322–4327 Å.

Table 11
Observed and the Predicted CNO Abundances for the Program Stars

Stars	[Fe/H]	Log ϵ(O)	Δ[a]	Log ϵ(N)	log ϵ(C)	Log ϵ(N)$_{predicted}$		[(C + N + O)/Fe]$_{obs}$	Log ϵ(Li)	He/H
						Log ϵ(C+N)$_0$	Log ϵ(C+N+O)$_0$			
Sun	0.0	8.69	⋯	7.83	8.43	⋯	⋯	8.91	1.05	0.1
KIC 5184199	−0.05	8.87	0.18	8.0	8.27	8.47	8.86	0.15	<0.50	0.1
KIC 12645107	−0.10	9.0	0.32	8.3	7.88	8.42	8.81	0.29	3.72	0.1
HR 6766	−0.05	8.73	0.09	8.67	7.45	8.45	8.85	0.14	1.18	0.1
KIC 9821622	−0.5	8.84	0.65	8.26	8.15	8.00	8.40	0.60	1.54	0.1
Ups02 Cas	−0.4	8.72	0.03	7.7	8.11	8.12	8.51	0.46	<−0.3	0.1
KIC 2305930	−0.40	9.5	0.81	7.8	8.11	8.12	8.51	1.01	4.03	0.4
HD 19745	0.0	8.60	−0.13	7.4	8.5	8.50	8.90	0.0	4.55	0.1
HD 40827	−0.1	9.07	0.38	8.30	8.47	8.40	8.80	0.42	1.87	0.1
HD 214995	−0.1	8.95	0.36	8.15	8.50	8.40	8.80	0.31	3.27	0.1
HDE 233517	−0.25	9.34	0.65	8.1	8.25	8.25	8.65	0.81	4.24	0.1
HD 107484	−0.15	9.04	0.35	8.1	8.44	8.40	8.76	0.141	2.10	0.4
HR 334	0.04	8.85	0.12	7.55	8.65	8.54	8.94	0.31	1.37	0.1
HR 4813	0.04	8.84	0.13	7.55	8.70	8.54	8.94	0.38	<−0.2	0.1
HD 112127	0.07	8.95	0.21	7.85	8.8	8.57	8.97	0.23	3.4	0.4
Arcturus	-0.6	8.75	0.06	7.45	8.15	7.92	8.31	0.58	<−1.0	0.1
HD 205349	−0.25	8.85	0.41	7.80	8.6	8.25	8.65	0.30	1.92	0.1
HD 77361	0.0	8.75	0.06	7.4	8.7	8.50	8.90	0.21	3.90	0.4
HD 30834	−0.18	8.5	−0.03	7.05	8.18	8.32	8.72	1.36	2.3	0.3
HD 181475	0.1	9.1	0.31	7.40	8.7	8.60	9.00	0.11	<−0.80	0.5
HD 39853	−0.20	8.53	0.0	7.5	8.5	8.32	8.71	1.47	3.90	0.1

Note. log ϵ(C + N)$_0$ and log ϵ(C + N + O)$_0$ are the predicted N abundances for the CN- and CN+ON-cycles from the stars' initial CNO abundances.
[a] $\Delta = \log(\epsilon(O)_{obs}/\epsilon(O)_0)$.

7.1. Results

7.1.1. He-rich Stars

The results are discussed in the light of Li, He, and CNO abundances for program stars among other available elemental abundances. KIC 2305930 is an RC star with the derived He/H and [Fe/H]$_{He}$ ratios of 0.4 and −0.6, respectively, the star is not only He enriched but also a super-Li rich with $\log \epsilon$ (Li) = 4.03 dex. The abundance ratios are [C/Fe] = 0.06, and [N/Fe] = +0.35 and the ^{12}C/^{13}C = 6. The observed O-abundance ratio is about [O/Fe] = +1.19 dex. For giants, the observed [O/Fe] is about +0.4 (C. Sneden 1991 and

references therein), and [O/Fe] of up to +1.0 has been observed for dwarfs (C. Abia & R. Rebolo 1989) of solar and near solar metallicity, and possibly increasing with decreasing metallicity. Here, the measured O-abundance plausibly represents the pristine material's O-abundance from which the star is formed. Table 11 shows the observed abundance of CNO, and the Δ here denotes the difference between the observed and the predicted initial O-abundance for the star's metallicity. If only the CN-cycle is operating, then the predicted N abundance for the initial C and N abundances is given by (C+N)$_0$, and if the CN- and ON-cycle is operating, the N abundance predicted for the initial composition of C, N,
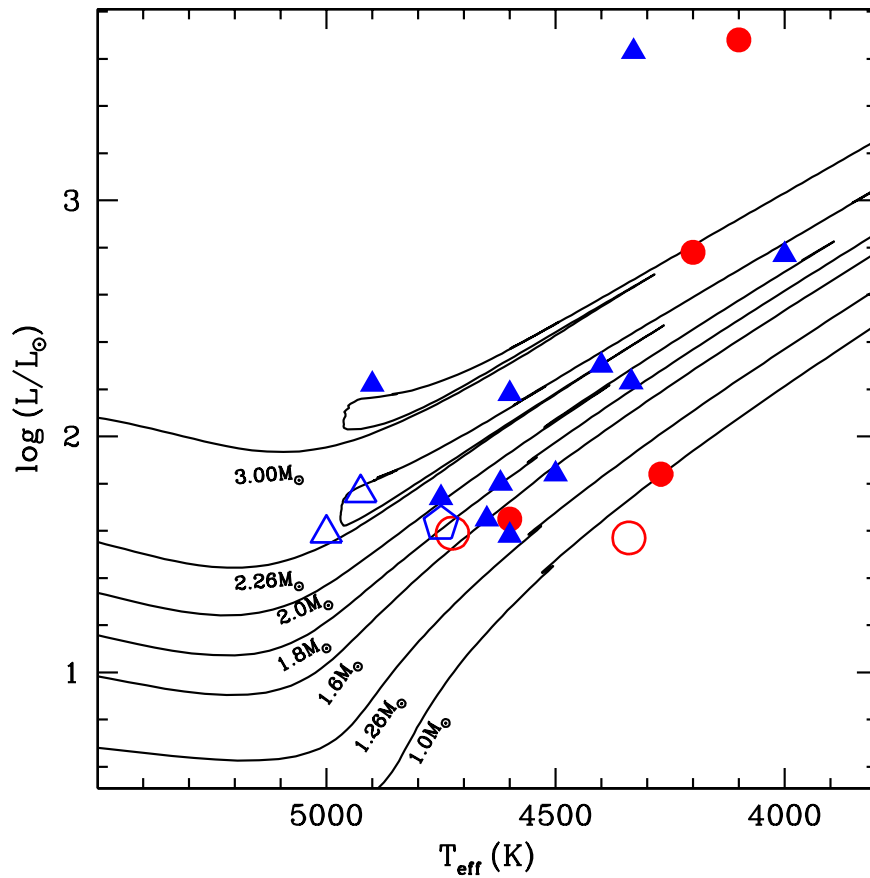
Figure 10. HR diagram for the program stars—the luminosity ($L_\odot$) vs. the T_{eff}. The blue solid triangles are the He-normal giants and the red dots are the He-enriched giants. The open triangles are the He-normal RC stars and red circles are the He-enriched RC stars from Kepler data. The open pentagon is an RGB-bump star: KIC 9821622 from Kepler data.

and O are given by $(C+N+O)_0$. The observed N abundance for KIC 2305930 is about 7.8 dex, which is close to the predicted N abundance of $(C+N)_0$ of 8.12 dex. Considering this as within the uncertainties, the C, N, and C isotopic ratios suggest that the surface composition is as expected for the first dredge up. Along with these quantities, the enrichment is also observed for He as well as Li. This high enrichment in Li, as mentioned above, would require fresh synthesis along with the preservation of the pristine Li with which the star is formed. The initial/primordial Li abundance is almost constant, i.e., $\log \epsilon(Li) = 3.3$ dex, for the metallicity ranging from $-0.5 <$ [Fe/H] $< +0.2$ dex (D. L. Lambert & B. E. Reddy 2004; S. Randich et al. 2020). The MS Li abundance is expected to be diluted up to ≈ 1.9 to 1.6 dex for the mass range of $1M_\odot$ to $1.5M_\odot$ by the time they arrive at the base of the RGB phase. If the original Li abundance with which the star is formed is less than the primordial value, then the abundance of Li during the RGB phase would further decrease. KIC 2305930 is also a binary star (A. Jorissen et al. 2020), which might have contributed by its binary companion in the enhancement of He and Li during mass-loss and mass transfer. Like in other program stars, La does not show any enhancement, indicating that the companion is not an AGB star or that it has not gone through the AGB phase.

HD 107484, by its position on the HR diagram, is probably at the tip of the RGB. From Table 11, the observed N abundance is about 8.1 dex, which is close to the N abundance predicted for $(C+N)_0$ of 8.4 dex, within the uncertainties. This indicates that the surface composition is as expected for the

first dredge up with the enhancement in He as well as Li (see Table 6). Based on the criteria suggested by R. de la Reza (2025), the derived $\log g$ of about 2.5 cm s^{-2} for HD 107484 is like an RC star. The La is found to be moderately enhanced, but no information on the binarity is available.

HD 112127 is an RC star with He enrichment of about He/H = 0.4 for [Fe/H]$_{He}$ = -0.4 and $\log \epsilon(Li) = 3.4 \pm 0.1$ dex. The abundance ratios are [C/Fe] = 0.30, and [N/Fe] = -0.05 and the $^{12}C/^{13}C$ = 22, as expected. The observed N abundance is about 7.85, which is very different from that predicted for CN- and ON-cycled N abundance, which are 8.57 and 8.97 dex, respectively (see Table 11). However, the $^{12}C/^{13}C$ ratio is less than that observed in the MS stars, suggesting surface enrichment with the dredge-up material. This would involve both preserving and fresh synthesis of Li, which is brought to the surface along with He and ^{13}C. The enhancement in La is the same as that observed in HD 107484, with no information on binarity.

For HD 77361, the He enhancement is about 0.4 for [Fe/H]$_{He}$ = -0.3 dex, with $\log \epsilon(Li) = 3.90$ dex. The derived N abundance, $\log \epsilon(N) = 7.4$ dex is very different from that predicted by CN and ON-cycle: 8.5 and 8.9 dex, respectively (see Table 11). The Li abundance of HD 77361 is greater than that expected in the MS phase. This requires the dredge up of freshly synthesized Li. The derived $^{12}C/^{13}C$ ratio is about 8, which is close to the equilibrium value of 3.4 and as expected. The C and N are not the absolute indicators of mixing/dredge up unlike the $^{12}C/^{13}C$ ratio along with He and Li enhancement. The effective mixing observed could be due to the processes that take
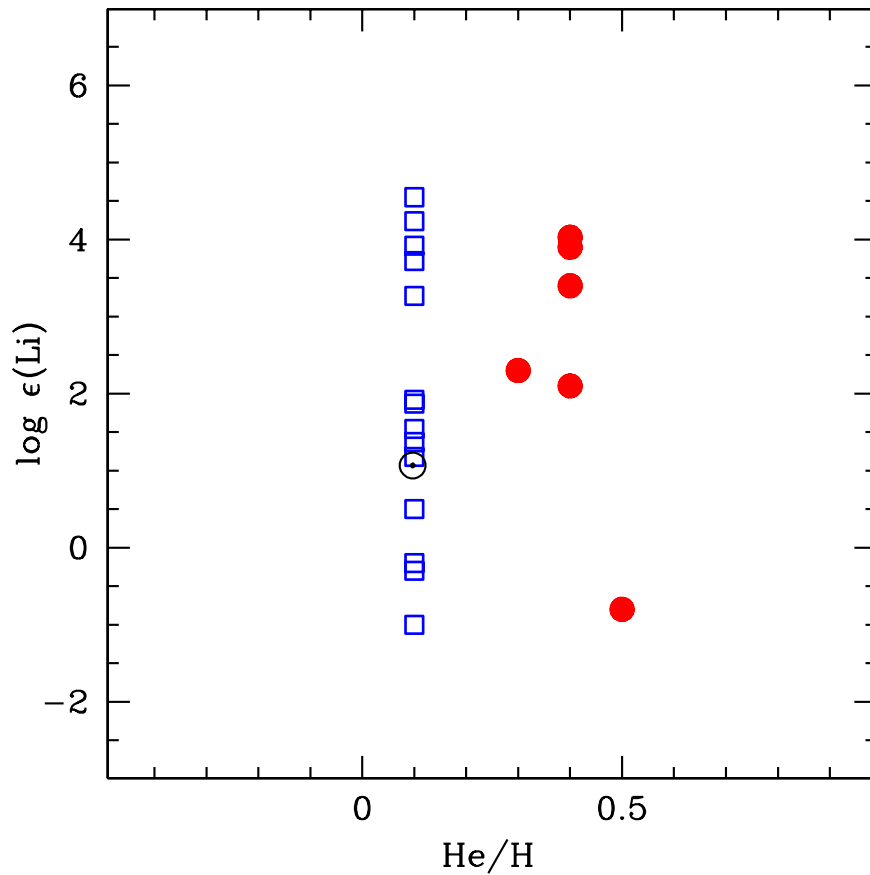
Figure 11. The Li-abundance, log ϵ(Li), for the program stars vs. the (He/H). The open blue squares are the stars with normal He/H ratios (He/H = 0.1) and the filled red circles are the He-enhanced ones (He/H > 0.1).

place in the bump phase of the RGB stars. The La is highly enhanced, indicating that the atmosphere is polluted by an AGB companion. However, no information on the binarity is available for the program star. According to the criteria of R. de la Reza (2025), the log g does not fall in both RGB or RC group.

HD 30834 is an early-AGB star with He enhancement of about 0.3 for [Fe/H]$_{\mathrm{He}}$ = −0.45 dex and log ϵ (Li) = 2.30 dex. The abundance ratios are [C/Fe] = −0.07, [N/Fe] = −0.6, [O/Fe] = 0.04, and the ^{12}C/^{13}C = 13. The derived N abundance, logϵ(N) = 7.05 dex, is very different from that predicted by CN- and ON-cycle, respectively (see Table 11). The depletion in nitrogen is not as expected for the red giants but this would be the effect of either conversion of N to Ne on AGB (A. I. Karakas & J. C. Lattanzio 2003) or N may be less in the material with which the star is formed. Hence, the Li , He, and the ^{13}C enrichment suggest mixing. The mass of HD 30834 is relatively higher (M = 4.5$M_\odot$) compared to other program stars. Once the He in the core has been exhausted, the star's ascent on the AGB begins. In the AGB phase, the convective envelope deepens, reaching the maximum depth, and connecting the He-rich layer. This would trigger the production of Li by the Cameron–Fowler process, as discussed in C. Charbonnel & S. C. Balachandran (2000). However, the observed Li abundance and the ^{12}C/^{13}C ratio are similar to other program stars because a thin hydrogen shell burning would only commence by the end of the early-AGB phase followed by the thermally pulsating phases. Hence, the derived abundances in the early-AGB stars are similar to those

observed in the RGB stars. The [La/Fe] shows enhancement, which is as expected for an AGB star.

HD 181475 is a supergiant star enhanced in He. This star is He enriched but not Li rich, unlike the other He-enriched program stars discussed above. The Li abundance is about log ϵ (Li) = −0.8 dex. The abundance ratios are [C/Fe] = 0.16, and [N/Fe] = −0.54. The ^{12}C/^{13}C ratio could not be derived for the star because the spectra did not cover the CN-band at about 8000 Å. From Table 11, the observed N abundance is about 7.4, which is very different from that predicted for (C+N)$_0$ = 8.6 and (C+N+O)$_0$ = 9.0 dex, respectively. Since this is a supergiant, there would be multiple episodes of convection and mixing happening, which would result in the He enhancement and Li depletion.

The He- as well as Li-enhanced giants have been discussed above, but we also observe stars that are Li rich but not He rich. The majority of our sample stars have a range in Li abundance: no-Li, Li rich, and super-Li rich, with no He enhancement. The program stars that have no-Li, with logϵ (Li) ⩽ 1.00 dex are KIC 5184199, Ups02 Cas, HR 4813, and Arcturus. The stars that have logϵ(Li) ⩾ 1.18 dex are grouped as Li rich, they are HR 6766, KIC 9821622, HD 40827, HR 334, and HD 205349. The giants with logϵ(Li) ⩾ 2.5 dex are grouped as super-Li rich, they are KIC 12645107, HD 19745, HD 214995, HDE 233517, and HD 39853. A discussion of these three groups are as follows.
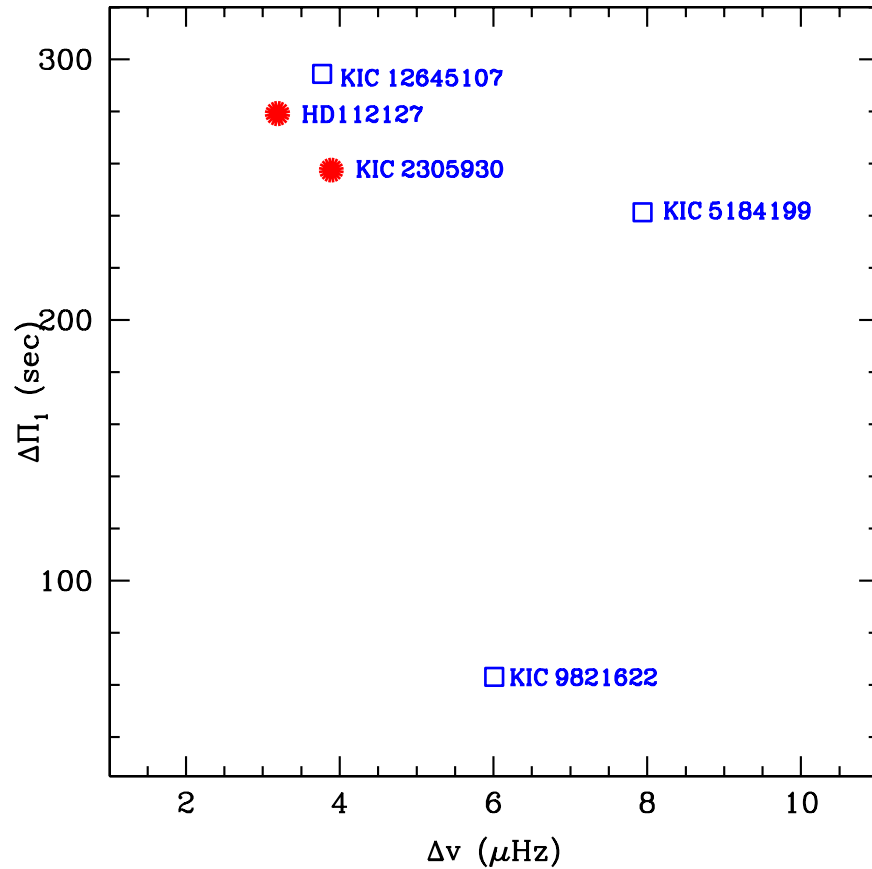
Figure 12. A plot of $\Delta\Pi_1$—$\Delta\nu$ for the programs stars with known evolutionary states using asteroseismology. The open blue squares are the giants with normal He/H ratio (0.1) and the filled red circles are the giants with He enhancement.

7.1.2. Giants with No/Minimal Li

Our sample giants, KIC 5184199, Ups02 Cas, HR 4813, and Arcturus , have no/minimal Li, having the $\log\epsilon(\text{Li}) \leqslant 1.00$ dex and $^{12}\text{C}/^{13}\text{C} < 25$, as expected. Though these stars have different [C/Fe] and [N/Fe] abundance ratios, indicating different scales of mixing, their Li and $^{12}\text{C}/^{13}\text{C}$ ratios are as expected for the first dredge up in RGB stars. Hence, $^{12}\text{C}/^{13}\text{C}$ is a better indicator of mixing. For these stars, the derived N abundance is not as predicted for the CN-cycling (see Table 11).

7.1.3. Li-rich Giants

Another subgroup is with Li-rich abundance $1.18 < \log\epsilon(\text{Li}) < 2.5$. These are HR 6766, KIC 9821622, HD 40827, HR 334, and HD 205349. Among these giants, HR 6766, KIC 9821622, and HD 40827 show efficient mixing with greatly enhanced N and depleted C, unlike the other two stars, HR 334 and HD 205347 (see Table 11). Surprisingly, despite high enhancement in N and highly depleted C in the weak *G*-band star, HR 6766, the Li is measurable and like that of an MS star. This is a puzzle, is this Li preserved or freshly synthesized? The observed abundances in KIC 9821622 and HD 40827 pose the same problem as well. The other two giants, HR 334 and HD 205349, neither show efficient mixing nor Li depletion completely (see Table 11)—indicating that Li here is preserved from the MS phase.

7.1.4. Super-Li-rich Giants

This is a group of giants with super-Li-rich abundances with no He enhancement, and these are KIC 12645107, HD 19745, HD 214995, HDE 233517, and HD 39853. KIC 12645107 is an RC star with [C/Fe] $= -0.45$ and [N/Fe] $= 0.57$. The $^{12}\text{C}/^{13}\text{C}$ ratio is about 6, with $\log\epsilon(\text{Li}) = 3.72 \pm 0.1$ dex. The observed N abundance $(\log\epsilon(\text{N}) = 8.3$ dex) is similar to that predicted for the CN-cycled abundance $(\log\epsilon(\text{N}) = 8.42$ dex). These abundances are as expected for giants except for Li, which is similar to the primordial value. For the other giants of this sample, the observed N abundance is similar to that predicted for CN-cycling (refer to Table 11), as expected, except for HD 19745 and HD 39853. The super-Li-rich abundance is probably the result of preservation from the pristine material or/and the fresh synthesis in these stars.

7.2. Discussion

As discussed above, our sample stars belong to different stages spanning from the base of the RGB to the early-AGB phase. The metallicity of the sample is $-0.6 < $ [Fe/H] $< +0.2$ dex. The main aim of this study is the investigation of photospheric He enhancement in principle, along with the CNO abundances and the $^{12}\text{C}/^{13}\text{C}$ ratio, in tandem with their Li abundances. The main discovery of this work is that all the He-enhanced red giants, including an early-AGB star, are super-Li rich, except for the supergiant star. This indicates that the photospheric He enrichment is accompanied by the Li enrichment in the giants, as we envisage. Our Li-rich sample stars evince that two or more processes, at least, are responsible for Li enrichment in
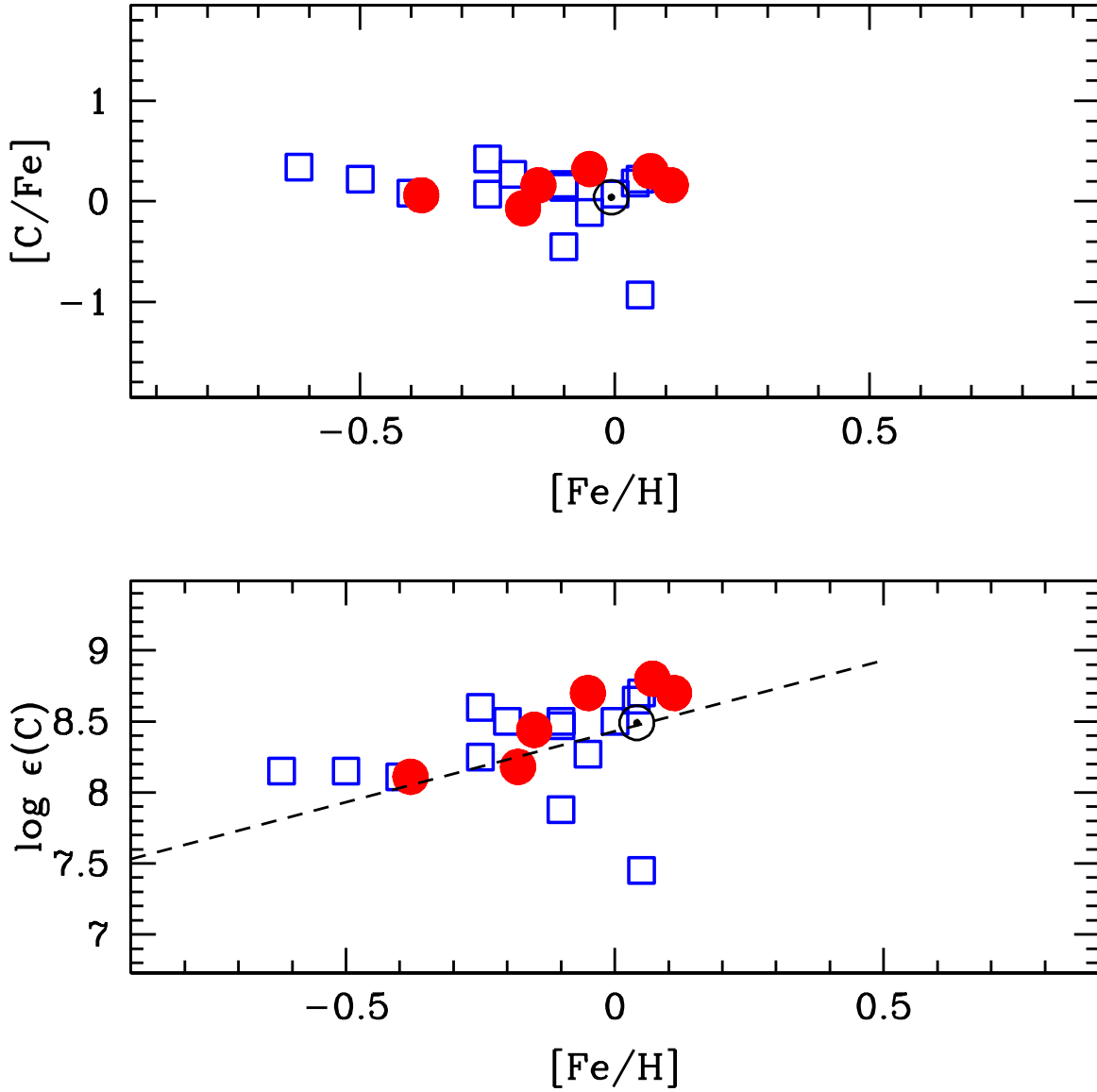
Figure 13. Bottom panel: The abundance of carbon derived for the program stars vs. [Fe/H]. The open blue squares are the giants with normal He/H ratio (0.1) and the filled red circles are the giants with He enhancement. The dashed line is for the initial carbon with respect to metallicity and $\odot$ represents the Sun. Top panel: The C abundance relative to Fe, w.r.t. Sun, [C/Fe] for the program stars vs. [Fe/H]. The open blue squares are the giants with normal He/H ratio (0.1) and the filled red circles are the giants with He enhancement, and $\odot$ represents the Sun.

giants: one to enrich only Li, and another to enrich He along with Li.

A. Mallick et al. (2025) report the correlation between the high photospheric Li abundances and the strong chromospheric He I $\lambda10830$ Å absorption line strengths in Kepler field giant stars. The correlation of high photospheric Li abundance with the strong chromospheric He I line is found exclusively among RC giants. Our results show that the high photospheric Li abundances are in correlation with the photospheric He enrichment. We looked for the equivalent width of the He I line for our program stars in their sample, and found two stars in common with their study. These are Li-rich RC stars, KIC 2305930 and KIC 12645107. In our study, we find that one, KIC 12645107, is a He normal and another, KIC 2305930, is He enhanced. The He-enhanced KIC 2305930 has a strong He I line $\lambda10830$ Å of $EW_{He} = 300 \pm 10$ mÅ with $\log \epsilon(Li) = 4.03$ dex, while the He-normal KIC 12645107 has a moderately strong He I line at $\lambda10830$ Å of

$EW_{He} = 95 \pm 8$ mÅ with $\log \epsilon(Li) = 3.72$ dex. For these two stars, relatively, it is observed that the chromospheric $\lambda10830$ Å He I line is more pronounced in the He-enriched star than in the He-normal one. This is an indication that the chromospheric He activity in RC stars is correlated with the photospheric He enhancement with confirmed super-Li-rich abundances.

However, as observed from our results, He enhancement is not only confined to RC stars but also observed in RGB stars. Our five He-rich RGBs include two RC stars, one from the RGB tip and another from the RGB-bump phase along with an early-AGB star. Since the lifetimes of the RC phase are two to five times longer than the RGB phase (I. J. Iben 1967), it is likely to find more RC stars with only Li enrichment as well as both He and Li enrichment. Further studies on a significant sample including both the RC and RGB samples with known evolutionary states would help to discern the scenarios responsible for these observations.
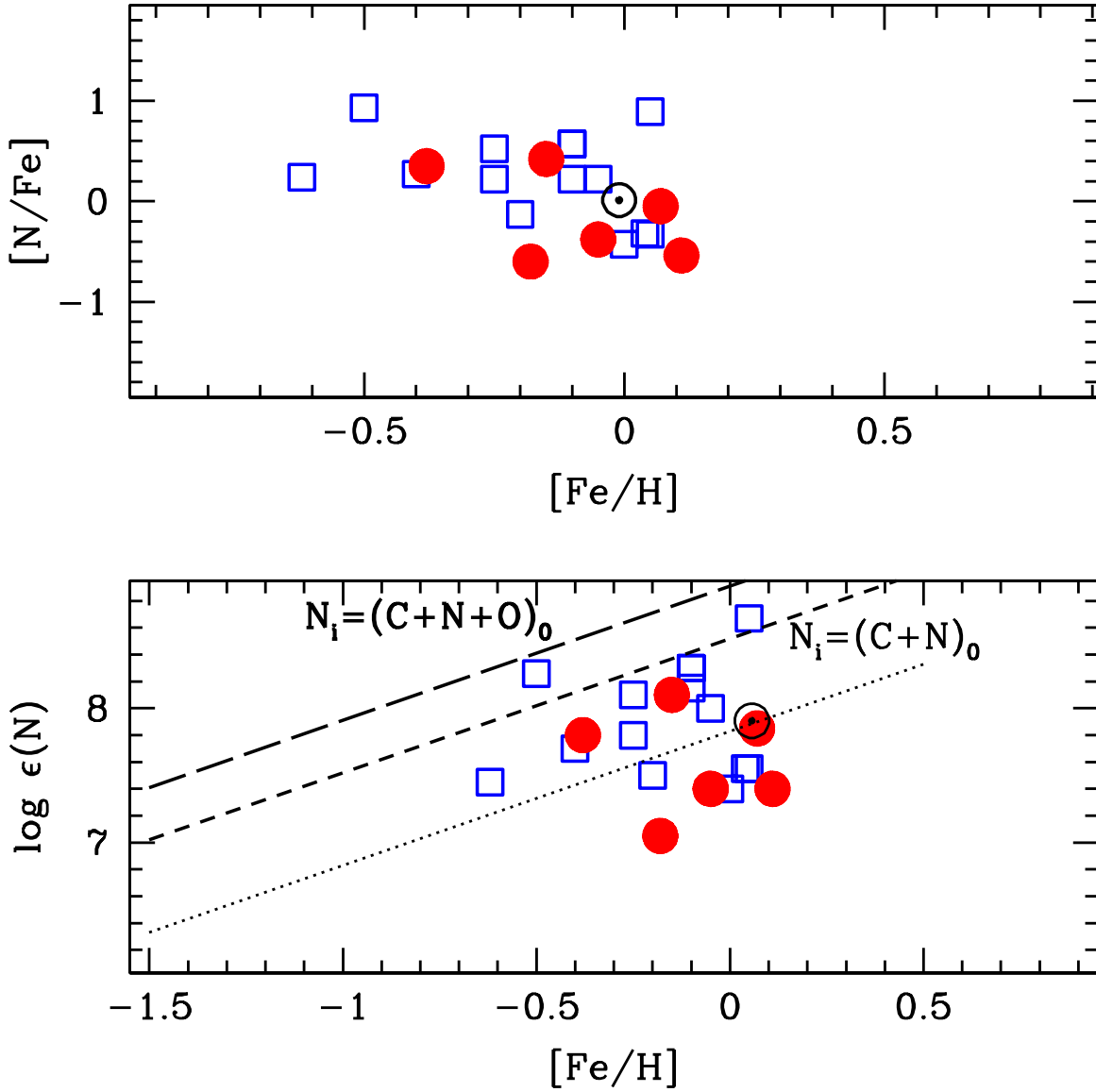
Figure 14. Bottom panel: The abundance of Nitrogen (log ϵ(N)) derived for the program stars vs. [Fe/H]. The open blue squares are the giants with normal He/H ratio (0.1). The filled red circles are the giants with He enhancement. The short-dashed line for $\log\epsilon(N)_i = (C+N)_0$, and the long-dashed line for $\log\epsilon(N)_i = (C+N+O)_0$, where $\log\epsilon(N)_i$ is for CN- and ON-cycles for initial CNO abundances, with [Fe/H] the metallicity as denoted. Top panel: The abundance ratio of Nitrogen, [N/Fe] derived for the program stars vs. [Fe/H]. The open blue squares are the giants with normal He/H ratio (0.1) and filled red circles are the giants with He enhancement, and $\odot$ represents the Sun.

The derived CN abundances of the program stars show no uniformity. The relation of $\log \epsilon$(C) and $\log \epsilon$(N), and their abundance ratios versus [Fe/H] for the program stars are shown in Figures 13 and 14, respectively. However, the ^{12}C/^{13}C ratios derived for the sample giants, i.e., $\leqslant 22$, is as expected for giants. The low-mass sample giants with the $M \sim M_\odot$ are expected to operate only the pp-chain in their interiors during their MS phase. Hence, the processed material, especially CNO, that is brought to the surface during the dredge up is almost similar to the primordial/MS composition. This is as observed in some of our program stars. A few program stars are intermediate-mass stars that operate CN-cycle along with the pp-chain at the center during the MS phase. This material that is enriched with CN-cycled material is dredged up and mixed with the surface (D. D. Clayton 1968; A. R. Choudhuri 2010).

Out of six He-enriched giants of our study, two giants show enhancement in N as expected for CN-cycle. However, in the top panel of Figure 15, with [C/N] versus $\log \epsilon$(Li) relation, the [C/N] ratio shows a nearly constant trend that is less than the solar value, suggesting C depletion and N enhancement relative to Fe, with respect to solar. The He-rich stars are in the super-Li-rich regime in the luminosity versus Li relation, as shown in the bottom panel of Figure 15. The other elemental abundances derived for the program stars are as expected for the giants with about nine program stars showing enhancement in La from 5 to 10 times solar. The He-enhanced giants, HD 77361 and HD 30834 show enhancement in La abundance with [La/Fe] ~ 1.0 dex. HD 112127 and HD 107484 show only moderate enhancements in [La/Fe]. The [La/Fe] is like solar for KIC 2305930, and the supergiant star shows a very high enhancement of about [La/Fe] = 1.45 dex, as expected for an AGB star. Out of the He-normal giants, about 10 giants
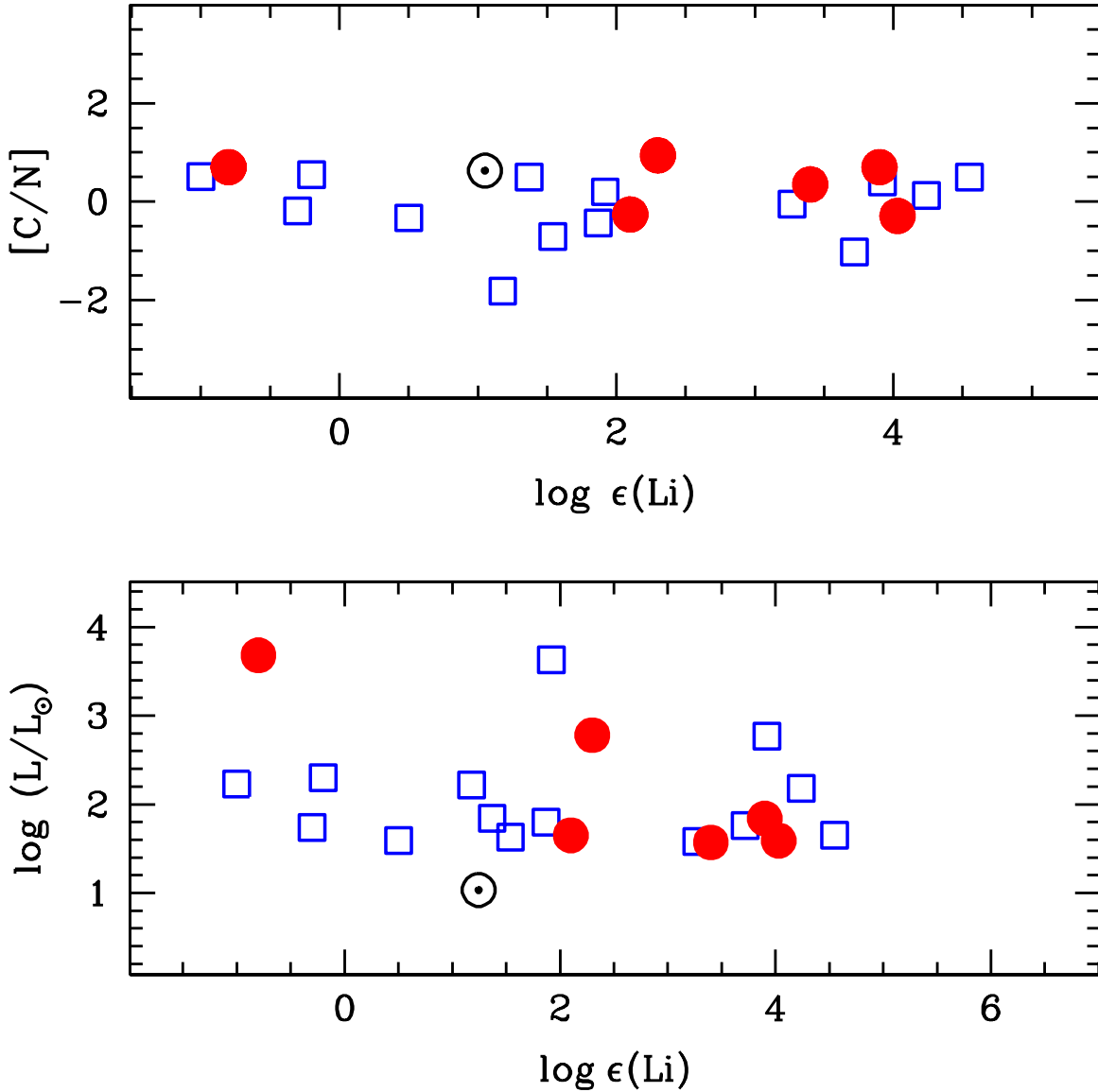
Figure 15. Bottom panel: The luminosity ($L/L_\odot$) vs. the Li-abundance, log ϵ(Li), for the program stars. The blue open squares are the stars with normal He/H ratios and the filled red circles are the He-enhanced ones. Top panel: The ratio of C and N w.r.t. Sun [C/N] vs. the Li abundance for the program stars. The open blue squares are the stars with normal He/H ratio (=0.1) and the filled red circles are the He-enhanced ones.

show moderate enhancement and other four of them show no enhancement in [La/Fe]. Since our La abundance is from a single line, we do not draw any conclusions based on this measurement.

Multiple scenarios are proposed to explain the Li enrichment in giants. First, preserving the Li from the pristine (if different from primordial) material with which the star is formed. Second, the fresh production of Li during the MS and RGB that is brought to the surface through the convection and dredge up. The third efficient channel for Li enrichment is via planet engulfment.

As the star evolves off the MS phase and moves along the giant branch, its core shrinks and the outer envelope expands engulfing its nearest planets. For example, the Earth has Li that is one to two orders greater than that observed in the Sun (J. B. Alexander 1967). If a giant engulfs an Earth-like planet, the host star becomes Li rich. In the atmosphere of a Jupiter-like planet, the Li is diluted and the helium is enhanced ((He/H2) = 0.16 ± 0.03 L. Ben-Jaffel & F. Herbert 2010).

Such planets do not change the Li abundance in the atmosphere of the host star on engulfment (J. B. Alexander 1967). However, for a giant to become Li rich on engulfing a planet, the mass of the giant/host star as well as the mass of the planet are crucial.

In this work, the most probable scenario that is deemed apt for the five He- as well as Li-enriched giants would be the fresh production of Li in the interiors of the RGB stars that is swiftly dredged up to the surface along with He from the deeper layers (C. A. Pilachowski et al. 1990).

These plausible scenarios of how the Li survives from the hotter temperatures need to be addressed. In addition, during the Cameron–Fowler reaction, we need to explore how the ^{7}Be is transported to cooler regions such that the ^{7}Li produced by the decay of ^{7}Be can survive (C. Charbonnel & S. C. Balachandran 2000; J. Gao et al. 2022). In this study, it is observed that all the He-enhanced red giants are super-Li rich, but all the Li-rich/super-Li-rich giants are not He rich. Y. B. Kumar et al. (2020), in their study of a large sample of giants, suggest that

all the low-mass stars undergo a lithium production phase between the tip of the RGB and the RC phase (see their Figure 3). Their findings suggest a new limit for Li enrichment in RC stars (the evolutionary states are determined from asteroseismology), i.e., $\log \epsilon(\text{Li}) > -0.9$ dex. However, as reported in many studies (mentioned above), including this work, giants show significant Li enrichment all across the giant branch for which the evolutionary states may or may not be determined solely from asteroseismology. The notable derived Li abundances among the sample stars of known evolutionary states from asteroseismology are about <0.50 dex for KIC 5184199 (RC star), 3.72 dex for KIC 12645107 (RC star), 4.03 dex for KIC 2305930 (RC star), 3.4 dex for HD 112127 (RC star), and 1.54 dex for KIC 9821622 the bump star. The RGB-bump star KIC 9821622 shows the Li enrichment which is also reported by E. Jofré et al. (2015). This indicates that giants with Li enrichment are observed in the RGB bump, RGB clump, and as well as in other stages of RGB evolution.

8. Concluding Remarks

The primary objective of this work is to detect and measure the He enhancement in the photospheres of cool giants, and further investigate any connection of He enhancement with Li enrichment. The program stars comprise a random sample of giants: 16 RGB, two early-AGB, and two supergiants, with and without Li enrichment. With the help of the observed optical high-resolution spectra of the program stars, a detailed abundance analysis was carried out to determine the abundances of the key elements: He, Li, C, N, O, among many others including the C-isotopic ratios. Using the difference in the Mg abundances derived from the Mg I and the MgH lines, the He enhancement is explored. These are better features to measure He abundance than the C I lines and CH band for giants. Out of these sample giants, we identified about four red giants, an early-AGB star, and a supergiant star to be He enriched. Surprisingly, all these He-enhanced red giants along with the early-AGB star are super-Li rich as well, except for the supergiant. This is a clear suggestion that the He enhancement is accompanied by a significant amount of Li enrichment/production in red giants, including early-AGB stars. The photospheric He enhancements in these stars also appear to be associated with their chromospheric He activity. Our results show that the Li enrichment is not necessarily associated with He enhancement. This again suggests that there must be multiple channels that make a star Li rich. Compared to the giants, supergiants undergo structural changes that affect the surface chemical composition. Hence, observing no-Li in the atmosphere of the supergiants is as expected despite the He enhancement. This work strongly evinces the process of fresh synthesis of Li and dredging up to the surface in the giant phase for the observed Li enrichment as one of the channels. The depth of the convection zone would be the deciding factor for He enhancement during the dredge up. These sound observational results await more thorough stellar interior models.

Appendix
CNO Abundances for the Program Stars

To understand the evolution of stars on the giant branch, it is crucial to know the abundances of the key elements: carbon, nitrogen, and oxygen. For all our program stars, the carbon, nitrogen, and oxygen abundances are derived using both the atomic and molecular lines. The new atomic lines included in this work are given in Table A1.

Carbon: To derive the carbon abundance, the permitted and the forbidden lines were used.

The permitted lines used are: $\lambda\lambda$4775.91, 5052.17, 5380.34, 6587.60, 8335.15, 9603.03, 9850.34 Å. The forbidden [C I] line is: λ8727.12 Å. These C I lines are from the D. L. Lambert (1978), W. L. Wiese et al. (1996), C. Abia et al. (2012), R. E. Luck & D. L. Lambert (1981), and D. L. Lambert & L. M. Ries (1981). These studies have used these lines to determine the CNO abundances for Sun and the giants. Though the CI lines in the spectra of the program stars are weak, they are well represented. For all these lines, the equivalent widths were measured in the spectrum of Arcturus and the lines were inverted for deriving the log gf values knowing the accurate carbon abundance (I. Ramírez & C. Allende Prieto 2011; B. P. Hema et al. 2018). The derived log gf values are in good agreement with those given in W. L. Wiese et al. (1996).

For all the program stars, a minimum of two C I and maximum of eight lines (as listed above) were found, subject to the wavelength span of the spectrum. The C I that are very weak/within the noise level of the continuum were discarded. However, more weight is given to C I: λ5380.34Å and [C I]: λ8727.12Å lines because these are less blended and relatively stronger and well represented than other spectral lines of carbon. The carbon abundances derived in this study are in good agreement with those available in the literature, including for the Arcturus.
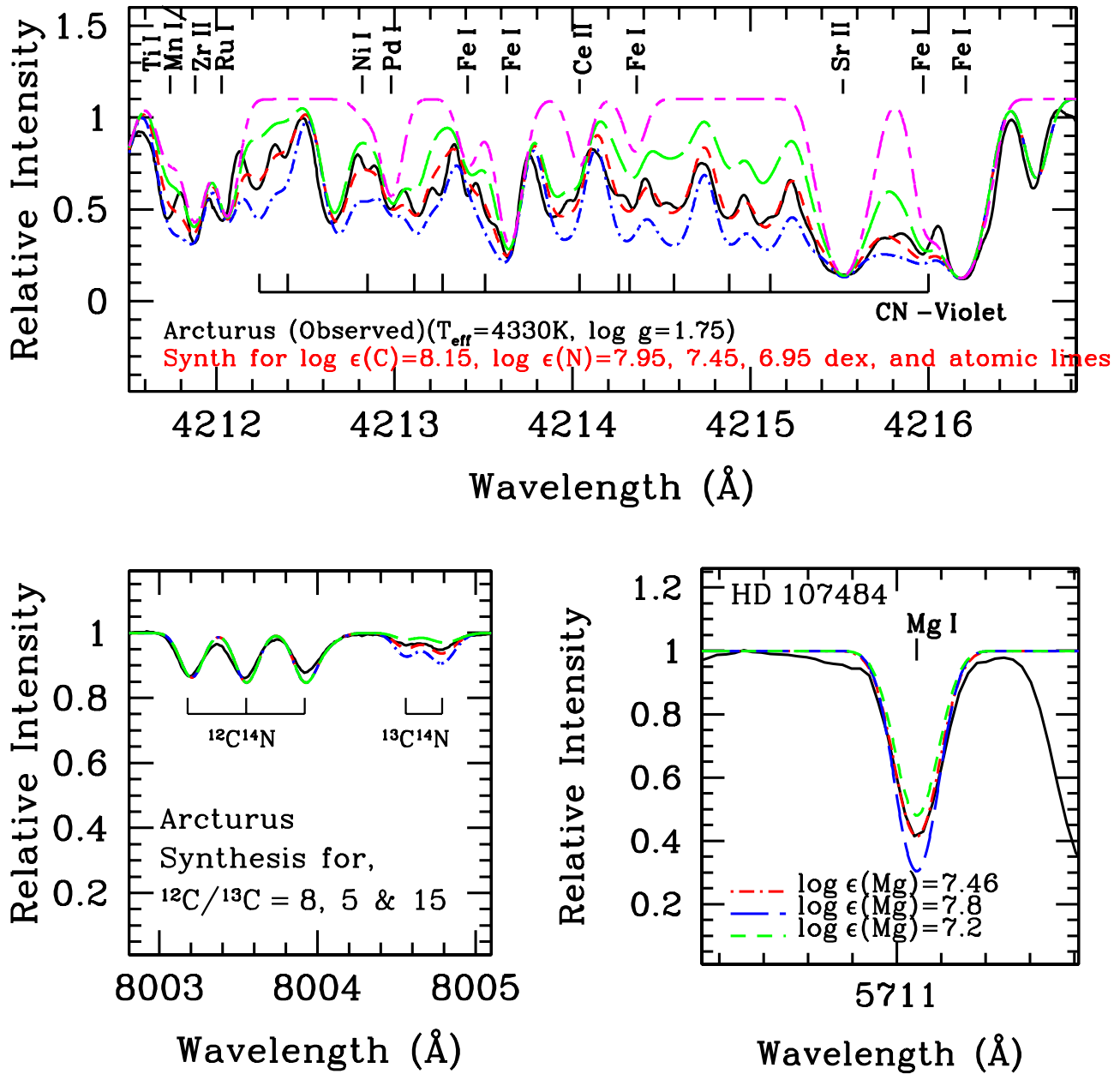
Figure A1. Top panel: The syntheses of the CN band for Arcturus. The synthesis shown with short-dashed red line is for the best fit N abundance. The syntheses are also shown for the other two values of N abundance for comparison, with long-dashed green line and dashed–dotted blue line. The long-short-dashed magenta line is for pure atomic lines. Bottom left: The determination of the $^{12}C/^{13}C$ ratio from $^{12}C^{14}N$ and $^{13}C^{14}N$, lines for Arcturus. The best fit is shown with the dashed red line for the $^{12}C/^{13}C = 8$, the synthesis for other two ratios are shown for comparison. Bottom right: The synthesis of the Mg I line, $\lambda\lambda5711$Å for the program star HD 107484, as an example.

Oxygen: To determine oxygen abundance in the program stars, the spectral lines used are:

The permitted lines: $\lambda\lambda6158.18, 9265.90, 7771.94, 7774.17,$ and 7775.39 Å.

The forbidden lines: $\lambda\lambda5577.34, 6300.30,$ and 6363.77 Å.

These lines are also from D. L. Lambert (1978), for which the log *gf* values are verified from the Solar and Arcturus spectrum. The derived log *gf* values are in good agreement with those from W. L. Wiese et al. (1996). The oxygen abundance derived in this study for Arcturus is in excellent agreement with that derived by I. Ramírez & C. Allende Prieto (2011) within the uncertainties. In the spectra of many of our program stars a minimum of three O I and two [O I] lines were present, allowing us to make a fair measurement of oxygen abundance.

Nitrogen: Several N I lines from the NIST database were compiled in the spectral range of the program stars. The N I lines have relatively higher LEP and are not expected to be seen in the cooler giants. The N I lines were not present in many of our program stars, but were present for a few giants with relatively warmer T_{eff} and significant enrichment in nitrogen. However, the best way to determine the nitrogen abundance is from the CN bands. For many of our program stars, the nitrogen abundance is derived from CN-red and CN-violet bands, as described below. Hence, using the program star's derived carbon abundance from C I lines, the nitrogen abundance was measured from the CN band.

CN band: The CN-red and CN-violet bands provide many weak and unblended lines, enabling the determination of

Table A1
The List of Newly Included Atomic Lines Along with Those Adopted by
B. P. Hema et al. (2018)

Species	λ (Å)	χ (eV)	log gf
Li I	6103.540	1.840	+0.106
Li I	6707.800	0.000	+0.020
C I	8335.150	7.680	−0.440
C I	9078.280	7.480	−0.570
C I	9111.800	7.490	−0.300
N I	7442.290	10.330	−0.330
N I	7468.310	10.340	−0.160
N I	8594.010	10.680	−0.320
N I	8683.400	10.330	+0.110
N I	8703.250	10.330	−0.290
N I	8718.830	10.340	−0.260
O I	7771.940	9.150	+0.330
O I	7774.170	9.150	+0.190
O I	7775.390	9.150	−0.030
Fe I	4635.850	2.845	−2.360
Fe I	4690.140	3.686	−1.640
Fe I	4802.880	3.642	−1.510
Fe I	5295.310	4.420	−1.590
Fe I	5329.990	4.070	−1.220
Fe I	5403.820	4.076	−1.030
Fe II	5414.070	3.221	−3.480
Fe I	5466.990	3.573	−2.23
Fe I	5483.100	4.154	−1.410
Fe I	5525.540	4.230	−1.080
Fe I	5661.348	4.280	−1.750
Fe I	5705.460	4.300	−1.360
Fe I	5741.850	4.256	−1.670
Fe I	5778.458	2.590	−3.450
Fe I	5784.661	3.400	−2.530
Fe I	5809.220	3.884	−1.610
Fe I	5849.69	3.695	−2.930
Fe I	5855.090	4.608	−1.480
Fe I	5856.100	4.294	−1.560
Fe I	5858.790	4.220	−2.180
Fe I	5859.600	4.550	−0.610
Fe I	5862.370	4.550	−0.250
Fe I	6027.060	4.070	−1.170
Fe I	6082.710	2.230	−3.550
Fe I	6159.380	4.610	−1.830
Fe I	6165.360	4.143	−1.460
Fe I	6271.283	3.330	−2.700
Fe I	6581.214	1.48	−4.680
Fe I	6591.330	4.593	−1.950
Fe I	6608.040	2.279	−3.910
Fe I	6713.750	4.795	−1.390
Fe I	6725.360	4.103	−2.170
Fe I	6733.150	4.638	−1.400
Fe I	6752.711	4.640	−1.200
Fe I	6793.260	4.076	−2.330
Fe I	6854.820	4.593	−1.930
Fe I	6857.250	4.076	−2.040
Fe I	7189.150	3.070	−2.770
Fe I	7401.690	4.186	−1.600
Fe I	7807.920	4.990	−0.510
Fe II	5234.620	3.221	−2.22
Fe II	5425.260	3.200	−3.160
Fe II	6149.250	3.889	−2.630
Fe II	6247.560	3.892	−2.270
Fe II	6369.460	2.891	−4.020
Fe II	6378.260	4.150	−1.050
Fe II	6432.680	2.891	−3.520
Fe II	6456.390	3.903	−2.060
Fe II	6516.077	2.891	−3.52

Table A1
(Continued)

Species	λ (Å)	χ (eV)	log gf
Fe II	7711.720	3.903	−2.450

Note. This table gives the species, wavelength (λ), LEP (χ), and the transition probabilities (log gf).

nitrogen abundance provided with an independent determination of the carbon abundance. The carbon abundances for the program stars are independently and accurately derived from the C I and [C I] lines. The nitrogen abundance has been mainly determined from the CN-violet system in the wavelength window: 4212–4217Å (see the top panel of Figure A1 for the synthesis of CN-band) and the ^{12}C/^{13}C ratio is determined from the CN-red system in the wavelength window: λ8000–8010 Å (see the bottom left panel of Figure A1 for deriving the ^{12}C/^{13}C ratio). This spectral window covers both the ^{12}C^{14}N as well as ^{13}C^{14}N lines. The line list for both red and violet bands were adopted from C. Sneden et al. (2014). By using the appropriate ATLAS9 (R. L. Kurucz 1998) model atmospheres with the MOOG synth code, the synthesized spectra were matched with the observed spectra of program stars by varying the nitrogen abundance and keeping the carbon abundance from the C I lines fixed. This data and procedure are validated by synthesizing the Arcturus spectrum. This derived nitrogen abundance from CN bands for Arcturus is in good agreement with that reported by C. Sneden et al. (2014) (see the bottom panel of Figure 3 therein) within the uncertainties.

ORCID iDs

B. P. Hema ⦿ https://orcid.org/0000-0002-0160-934X
Gajendra Pandey ⦿ https://orcid.org/0000-0001-5812-1516

References

Abdurro'uf, Accetta, K., Aerts, C., et al. 2022, ApJS, 259, 35
Abia, C., Palmerini, S., Busso, M., & Cristallo, S. 2012, A&A, 548, A55
Abia, C., & Rebolo, R. 1989, ApJ, 347, 186
Adamczak, J., & Lambert, D. L. 2013, ApJ, 765, 155
Afşar, M., Sneden, C., & For, B. Q. 2012, AJ, 144, 20
Alexander, J. B. 1967, Obs, 87, 238
Balachandran, S. C., Fekel, F. C., Henry, G. W., & Uitenbroek, H. 2000, ApJ, 542, 978
Ben-Jaffel, L., & Herbert, F. 2010, AGU Fall Meeting, 2010, P31A
Berdyugina, S. V., & Savanov, I. S. 1994, AstL, 20, 639
Bergemann, M., Lind, K., Collet, R., Magic, Z., & Asplund, M. 2012, MNRAS, 427, 27
Borisov, S. B., Chilingarian, I. V., Rubtsov, E. V., et al. 2023, ApJS, 266, 11
Borucki, W. J., Koch, D., Basri, G., et al. 2010, Sci, 327, 977
Brown, J. A., Sneden, C., Lambert, D. L., & Dutchover, E. J. 1989, ApJS, 71, 293
Cai, B., Kong, X., Shi, J., et al. 2023, AJ, 165, 52
Caldwell, D. A., Jenkins, J. M., & Ting, E. B. 2020a, TESS Light Curves From Full Frame Images ("TESS-SPOC"), STScI/MAST, doi:10.17909/T9-WPZ1-8S54
Caldwell, D. A., Tenenbaum, P., Twicken, J. D., et al. 2020b, RNAAS, 4, 201
Cameron, A. G. W., & Fowler, W. A. 1971, ApJ, 164, 111
Cayrel de Strobel, G., Crifo, F., & Lebreton, Y. 1997, in Proc. from the Hipparcos Venice '97 symposium, 402 ed. R. M. Bonnet et al. (Paris: ESA), 687
Ceillier, T., Tayar, J., Mathur, S., et al. 2017, A&A, 605, A111
Charbonnel, C., & Balachandran, S. C. 2000, A&A, 359, 563
Choudhuri, A. R. 2010, Astrophysics for Physicists (Cambridge: Cambridge Univ. Press)

Clayton, D. D. 1968, Principles of Stellar Evolution and Nucleosynthesis (New York: McGraw-Hill)
da Silva, L., de La Reza, R., & Barbuy, B. 1995, ApJL, 448, L41
de la Reza, R. 2025, A&A, 693, A98
de La Reza, R., & Drake, N. A. 1995, MmSAI, 66, 421
de La Reza, R., & da Silva, L. 1995, ApJ, 439, 917
de Medeiros, J. R., & Mayor, M. 1999, A&AS, 139, 433
de Medeiros, J. R., Melo, C. H. F., & Mayor, M. 1996, A&A, 309, 465
Deepak, & Reddy, B. E. 2022, ycat, 7484
Dekker, H., D'Odorico, S., Kaufer, A., Delabre, B., & Kotzlowski, H. 2000, Proc. SPIE, 4008, 534
Drake, N. A., de la Reza, R., da Silva, L., & Lambert, D. L. 2002, AJ, 123, 2703
Frasca, A., Guillout, P., Klutsch, A., et al. 2018, A&A, 612, A96
Gao, J., Zhu, C., Yu, J., et al. 2022, A&A, 668, A126
Gao, Q., Shi, J.-R., Yan, H.-L., et al. 2019, ApJS, 245, 33
Gonçalves, B. F. O., da Costa, J. S., de Almeida, L., et al. 2020, MNRAS, 498, 2295
Gratton, R. G., & D'Antona, F. 1989, A&A, 215, 66
Hema, B. P., & Pandey, G. 2014, ApJL, 792, L28
Hema, B. P., & Pandey, G. 2020, JApA, 41, 39
Hema, B. P., Pandey, G., Kurucz, R. L., et al. 2020, ApJ, 897, 32
Hema, B. P., Pandey, G., & Srianand, R. 2018, ApJ, 864, 121
Hinkle, K., Wallace, L., Valenti, J., & Harmer, D. 2000, Visible and Near Infrared Atlas of the Arcturus Spectrum 3727-9300 A (San Francisco, CA: ASP)
Hinkle, K. H., Wallace, L., Ram, R. S., et al. 2013, ApJS, 207, 26
Iben, I. J. 1967, ApJ, 147, 624
Jofré, E., Petrucci, R., García, L., et al. 2015, A&A, 584, L3
Jönsson, H., et al. 2020, AJ, 160, 120
Jorissen, A., Van Winckel, H., Siess, L., et al. 2020, A&A, 639, A7
Karakas, A. I., & Lattanzio, J. C. 2003, PASA, 20, 393
Kaufer, A., Stahl, O., Tubbesing, S., et al. 1999, Msngr, 95, 8
Kepler Mission Team 2009, ycat, 5133
Kumar, Y. B., & Reddy, B. E. 2009, ApJL, 703, L46
Kumar, Y. B., Reddy, B. E., Campbell, S. W., et al. 2020, NatAs, 4, 1059
Kumar, Y. B., Reddy, B. E., & Lambert, D. L. 2011, ApJL, 730, L12
Kumar, Y. B., Singh, R., Reddy, B. E., & Zhao, G. 2018, ApJL, 858, L22
Kurucz, R. L. 1998, http://Kurucz.harvard.edu/
Lambert, D. L. 1978, MNRAS, 182, 249
Lambert, D. L., Dominy, J. F., & Sivertsen, S. 1980, ApJ, 235, 114
Lambert, D. L., & Reddy, B. E. 2004, MNRAS, 349, 757
Lambert, D. L., & Ries, L. M. 1981, ApJ, 248, 228
Luck, R. E., & Challener, S. L. 1995, AJ, 110, 2968
Luck, R. E., & Heiter, U. 2007, AJ, 133, 2464
Luck, R. E., & Lambert, D. L. 1981, ApJ, 245, 1018
Lyubimkov, L. S., Kaminsky, B. M., Metlov, V. G., et al. 2015, AstL, 41, 809
Mallick, A., Sneden, C., Reddy, B. E., & Afşar, M. 2025, ApJ, 980, 265
Mallinson, J. W. E., Lind, K., Amarsi, A. M., et al. 2022, A&A, 668, A103
Martell, S. L., Simpson, J. D., Balasubramaniam, A. G., et al. 2021, MNRAS, 505, 5340
Mashonkina, L., Gehren, T., Shi, J. R., Korn, A. J., & Grupp, F. 2011, A&A, 528, A87
Mashonkina, L. 2024, MNRAS, 527, 8234
McWilliam, A., & Lambert, D. L. 1988, MNRAS, 230, 573
Moharana, S., Hema, B. P., & Pandey, G. 2024, ApJ, 974, 312
Moultaka, J., Ilovaisky, S. A., Prugniel, P., & Soubiran, C. 2004, PASP, 116, 693
Palacios, A., Jasniewicz, G., Masseron, T., et al. 2016, A&A, 587, A42
Palacios, A., Parthasarathy, M., Bharat Kumar, Y., & Jasniewicz, G. 2012, A&A, 538, A68
Pilachowski, C. A., Sneden, C., & Hudek, D. 1990, AJ, 99, 1225
Ramírez, I., & Allende Prieto, C. 2011, ApJ, 743, 135
Randich, S., et al. 2020, A&A, 640, L1
Reddy, B. E., & Lambert, D. L. 2005, AJ, 129, 2831
Reddy, B. E., Tomkin, J., Lambert, D. L., & Allende Prieto, C. 2003, MNRAS, 340, 304
Singh, R., Bharat Kumar, Y., Reddy, B. E., & Aoki, W. 2020, MNRAS, 491, 3838
Sitnova, T. M., Matsuno, T., Yuan, Z., et al. 2023, MNRAS, 526, 5976
Smiljanic, R., Franciosini, E., Bragaglia, A., et al. 2018, A&A, 617, A4
Sneden, C. 1991, in IAU Symp. 145, Evolution of Stars: the Photospheric Abundance Connection, ed. G. Michaud & A. V. Tutukov (Cambridge: Cambridge Univ. Press), 235
Sneden, C., Lucatello, S., Ram, R. S., Brooke, J. S. A., & Bernath, P. 2014, ApJS, 214, 26
Sneden, C. A. 1973, PhD thesis, The Univ. of Texas at Austin
Soto, M. G., Jones, M. I., & Jenkins, J. S. 2021, A&A, 647, A157
Sriram, S., Kumar, A., Surya, A., et al. 2018, Proc. SPIE, 10702, 107026K
Sumangala Rao, S., Pandey, G., Lambert, D. L., & Giridhar, S. 2011, ApJL, 737, L7
Tody, D. 1986, Proc. SPIE, 627, 733
Tody, D. 1993, in ASP Conf. Ser. 52, Astronomical Data Analysis Software and Systems II, ed. R. J. Hanisch, R. J. V. Brissenden, & J. Barnes (San Francisco, CA: ASP), 173
Tull, R. G., MacQueen, P. J., Sneden, C., & Lambert, D. L. 1995, PASP, 107, 251
Wallerstein, G., & Sneden, C. 1982, ApJ, 255, 577
Wiese, W. L., Fuhr, J. R., & Deters, T. M. 1996, Atomic Transition Probabilities of Carbon, Nitrogen, and Oxygen: A Critical Data Compilation (Washington, DC: American Chemical Society)